Universidade do Minho
Escola de Engenharia

Mariana de Sousa Fernandes

Photonic Platform for Bioelectric Signal Acquisition on Wearable Devices

Outubro de 2011

Mariana de Sousa Fernandes **Photonic Platform for Bioelectric Signal Acquisition on Wearable Devices**

UMinho | 2011

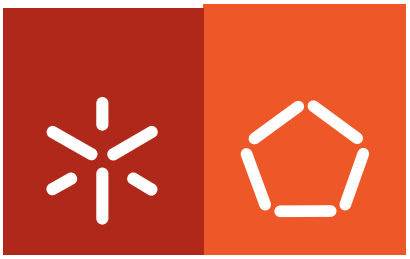

Universidade do Minho
Escola de Engenharia

Mariana de Sousa Fernandes

Photonic Platform for Bioelectric Signal Acquisition on Wearable Devices

Programa Doutoral em Bioengenharia

Trabalho realizado sob a orientação do
Professor Doutor Paulo Mateus Mendes
e do
Professor Doutor José Higino Correia

Outubro de 2011

Declaração

Nome
Mariana de Sousa Fernandes

Título da tese: Photonic Platform for Bioelectric Signal Acquisition on Wearable Devices

Orientador(es):

Professor Doutor Paulo Mateus Mendes
Professor Doutor José Higino Correia **Ano de conclusão**: 2011

Designação do Mestrado ou do Ramo de Conhecimento do Doutoramento:
Programa Doutoral em Bioengenharia

Universidade do Minho, 31 de Outubro, 2011

ACKNOWLEDGMENTS

It would not have been possible to run this marathon without the help and support of all the people that were around me, during the experience of pursuing my PhD. To all of them, I am truly grateful. Naturally, the names that will be mentioned here are those of the people that cannot be left unsaid – the special ones.

My foremost thank goes to my supervisor, Professor Paulo Mateus Mendes, for all his contributions of time, ideas, support and guidance to make my PhD a productive and stimulating experience. He has always helped me to become a more independent researcher and to think out of the box. The enthusiasm he has for his research was contagious and motivational.

An indebted thank to my co-supervisor, Professor José Higino Correia for his support and guidance and for giving me the pleasure of being his student and part of his research group.

I would also like to take this opportunity to express my appreciation to Professor Rajeev Ram for accepting me as a visiting student at his research group at MIT. It was a pleasure to be able to learn, discuss ideas and to be a part of his group. A special thanks, also, to my group colleagues, especially to Kevin Lee and Harry Lee for helping me with the research and for all the interesting brainstorming.

There is no doubt that I would have never been able to get with all the bureaucratic issues and questions regarding the MIT-Portugal Program without the help of Professor Eugénio Ferreira.

As a MIT-Portugal Program student, I had the privilege to become part of this network of professors, researchers and students. I strongly believe that this opportunity changed my way of facing research and prepared me for a new way of thinking. It was a pleasure to share my doctoral studies with my amazing colleagues from the Bioengineering focus area and to share all those crazy, funny and even stressful moments. A special thanks to Daniela Couto and João Guerreiro, my dearest friends and "10 Fulkerson" housemates. For the meals, the talks throughout the evening, the movies, the surprises..and most importantly, for being my family.

During the three years of lab work, I had the pleasure of the company of my laboratory colleagues Alexandre Ferreira da Silva, Amândio Barbosa, Carlos Pereira, Celso Figueiredo, Débora Ferreira, Helena Fernandez, João Ribeiro, Fábio Rodrigues, Doctor Luís

Rocha, Manuel Silva, Doctor Nuno Dias, Pedro Anacleto, Sérgio Dias, Susana Catarino Rosana Dias, Rui Rocha. To them I need to thank for the fun breaks we did, the ideias exchanged, the lunchs we all had together, as well as the Thursday and, sometimes, Friday's Cake day!

I am especially grateful to Alexandre Ferreira da Silva and Débora Ferreira that have been accompanying me since the beginning of my Academia adventure. Both of them had helped me as group colleagues, and mostly, as true friends. Without my endless talks with Débora and our crazy stories, it would have been much more difficult to surpass this challenge. To Alexandre, I have to thank not only for listening to my stupid jokes, ideas, questions, but also for the strong support that he has always been able to give me. Furthermore, without his equipment, most of the experiments herein described would not have been possible. "Double 02, where are you?". As I always say: "Alexandre, és um anjo, a minha salvação" ☺.

To the Industrial Electronics Department professors, technicians and secretaries, I express my gratitude for the availability of services. In particular, I would like to express my thankfulness to Professor Graça Minas, Professor Luis Rocha and Doctor Nuno Dias for providing some of the necessary equipment for the accomplishment of this PhD.

Now is the time of thanking all the beloved friends that helped me through this journey, either by sharing meals and coffees, watching movies, dancing, laughing, crying…everything. Frist, to my oldest, best and core friends, in particular Azz, Cris, Daniela, Betinha, Jonas, Jorge (my "brother" and my "pés-na-terra"), Liliana, Luisinho, Luis Carlos, Negras, Nhoca, Pãpã and Rui Pedro, Schroeder, Tiago, Renata and Valter thank you for being there and for all the patience and support.

I cannot proceed without saying a few words to some of them. Cris, Pãpã, Liliana thank you for being my best friends for a long long time. Each one of you contributed in a specific way, more than you can imagine. For you guys, our song "Amigos para sempre", with lyrics adapted, of course. And Daniela, I don't have the words..literally. Basically, you followed me (or vice-versa) in each step of our academia path, and always found a way to make me fell happier. From the first group works, to the last talks we had towards the end of writing this. Actually, right now I'm talking to you about not having words to describe how grateful I am. From the vast list of music we shared throughout these 4 years, I chose the one that always pushed us a step forward in thesis writing: *dance 'til you're dead, heads will roll.* Daniela, "Heads will Roll". Thank you for everything and how you always say "desculpa qualquer coisinha"

A new round of friends appeared, and since the group is almost 30 people, I will only mention a few names that cannot be forgotten, the funny guys: Gil, Manel, Mário, Mope and Zé. Thank you for all the fun moments, the dinners and the movies.

To my second family, D. Sameiro, Sr. Fernandes, Adriana e Luís, thank you for all the support and love. For welcoming me in your home and in your lifes as a member of your family, a thousand thanks.

Now the most important people for me, my partners in life and to whom I dedicate this thesis: my family and boyfriend. The best family in the world, from my grandparents to my little nephews! To my mother, father, sister, brother-in-law, my beloved nephews António and Rodrigo (as minhas perdições ☺), and Pedro, I cannot express how thankful I am. I feel like the luckiest person in this world to have you all in my life. Thank you for being there, for your unconditional love and support, for making me who I am, and for making this possible.

Pedro, the one that "suffered" the most, thank you for being unconditionally there as my boyfriend and my friend, right from the beginning of the most important years of my life. I owe you everything right now.

The final sentence should not be for anyone, but for my parents and my sister. They raised me, supported me, taught me, and, most of all, loved me unconditionally. A million times, thank you.

This work was supported by Portuguese Foundation for Science and Technology (SFRH/BD/42705/2007). The author would like also to acknowledge the MIT Portugal Program for supporting this work

ABSTRACT

Among all physiological functions, bioelectric activity may be considered one of the most important, since it is the backbone of many wearable technologies used for health condition diagnostic and monitoring. The existent bioelectric recording devices are difficult to integrate on wearable materials, mainly due to the number of electrical interconnections and components required at the sensing places. Photonic sensors have been presented in the medical field as a valuable alternative where features like crosstalk and attenuation, electromagnetic interference and integration constitute a challenge. Furthermore, photonic sensors have other advantages such as easy integration into a widespread of materials and structures, multiplexing capacity towards the design of sensing networks and long lifetime.

The aim of this work was to develop a multi-parameter bioelectric acquisition platform based on photonic technologies. The platform includes electro-optic (EO) and optoelectronic (OE) stages, as well as standard filtering and amplification. The core sensing technology is based on a Mach-Zehnder Interferometer (MZI) Modulator, which responds to the bioelectric signal by modulating the input light intensity. Only optical fibers are used as interconnections, and the subsequent signal conditioning and processing can be centralized in a common processing unit. The photonic and OE modules were designed to guarantee bioelectric signal detection using parameters compatible with existing technologies. Several considerations were made regarding noise-limiting factors, unstable operation and sensitivity. The EO modulator of choice was a Lithium Niobate ($LiNbO_3$) MZI modulator. The EO modulator was selected given its versatile geometry and potential to perform differential measurements and easiness to convert the resultant optical modulated signal into electrical values.

The OE conversion module developed includes a transimpedance amplifier (TIA), a notch and bandpass filter. In order to prevent a phenomenon called gain-peaking, the TIA was properly compensated, to insure a stable TIA operation and simultaneously avoid output signal oscillation. The performance of the TIA circuit was improved considering DC currents of 1.3 mA, which resulted in an additional high-pass filtering block. This allowed for a transimpedance gain of $1x10^5$ V/A. The filtering stage was designed for removing unwanted signal artifacts, and included two bandpass filters (0.2 – 40 Hz; 5 - 500 Hz) and a notch filtered centered at 50 Hz and with 34 dB of attenuation.

The photonic platform prototype performance was evaluated, covering linearity, frequency response and sensitivity. Results have shown that the combination of the photonic and OE stages had a flat 60 dB frequency over the frequency range of 0.3 Hz to 1 kHz. With regard to system linearity, it was verified a linear relationship between the voltage input and output signal, with a gain of 60 dB. These results indicated a correct biasing of the MZI modulator. In order to study the minimum detected fields that can be achieved using the developed prototype, the filtering and amplification stages were also considered. The characterization was performed with an overall gain of 4000 V/V (72 dB) and the photonic platform showed sufficient sensitivity to detect signals as low as 20 μV.

To assess the bioelectric signal acquisition performance, the developed photonic platform was tested in a real scenario through the acquisition of different bioelectric signals – Electrocardiogram (ECG), Electroencephalogram (EEG) and electromyogram (EMG). The results were compared with signals obtained from standard platforms using the same conditions. The developed photonic platform demonstrated the capability of recording signals with relevant and clinical content, providing enough sensitivity, frequency response and artifact removal. The photonic platform showed good results in various clinical scenarios, such as the evaluation of normal heart and muscle functions, as well as monitoring the consciousness state of patients.

As a final conclusion, a photonic platform for bioelectric signal acquisition was developed and tested; its application in wearable health systems was demonstrated.

RESUMO

De todas as funções fisiológicas, a actividade bioeléctrica é considerada uma das mais importantes, uma vez que representa a base para muitos sistemas vestíveis, utilizados para monitorização e diagnóstico no sector médico. Os dispositivos existentes - baseados em aquisição electronica - apresentam algumas desvantagens essencialmente relacionadas com a dificuldade de integração em materiais vestíveis, a quantidade de interligações e os componentes necessários nos locais de medição. Os sensores fotónicos têm vindo a ser cada vez mais utilizados no sector médico, uma vez que conseguem ultrapassar as desvantagens de atenuação e interferência electromagnética. Para além disso, este tipo de sensores apresenta uma fácil integração em diversos materiais, durabilidade e capacidade de multiplexagem, especialmente concebidas para redes de sensores.

O principal objectivo da presente tese foi desenvolver uma plataforma de aquisição de biopotenciais baseada em sensores fotónicos. A plataforma inclui um bloco responsável por efectuar a conversão electro-óptica (EO) do biopotencial medido, assim como a optoelectrónica (OE) necessária para transformar o sinal óptico para o domínio electrico.

A tecnologia que está na base do mecanismo de transdução desta plataforma consiste em moduladores Mach-Zehnder (MZI), cujo princípio é modular a intensidade da luz em resposta a um sinal electrico. As interconexões e transdução são efectuadas apenas por fibra óptica, sendo que o processamento e acondicionamento do sinal pode ser centralizado numa unidade de processamento transversal a todos os sinais.

Os módulos correspondentes aos blocos EO e OE foram desenvolvidos de forma a garantir a detecção do biopotencial utilizando características compatíveis com a tecnologia disponível. Foram efectuadas várias considerações relativamente aos factores que limitam o funcionamento adequado da plataforma fotónica, mais especificamente no que diz respeito a níveis de ruído, instabilidade e resolução. O modulador EO seleccionado foi um MZI de niobato de litio ($LiNbO_3$). A escolha deste modulador teve como principal motivo a possibilidade de efectuar medições diferenciais, geometria versátil e a facilidade de converter o sinal óptico resultante para o domínio eléctrico.

Os módulos de conversão OE desenvolvidos incluem um amplificador de transimpedância (TIA) e filtros passa-banda e notch. Para assegurar o funcionamento estável do TIA e evitar um fenóneno designado por *gain-peaking* (ganho de pico), foi necessário compensar devidamente o circuito. A performance do TIA desenvolvido foi optimizada para

currentes DC na ordem dos 1.3 mA, resultando na adição de um filtro passa-alto de forma a atingir ganhos de transimpedância de $1x10^5$ V/A. Os blocos de filtragem para remover as componentes de interferencia indesejados incluiram dois filtros passa-banda (0.2 – 40 Hz; 5 – 500 Hz) e um filtro notch centrado nos 50 Hz filtered e com um factor de atenuação de 34 dB.

O protótipo da plataforma fotónica, mais especificamente o modulo EO e OE (saída do TIA) foi submetido a diferentes testes com o principal objectivo de caracterizar o desempenho do sistema ao nível da resposta em frequência, linearidade e resolução. Os resultados obtidos demonstratam uma resposta em frequência com um agama dos 0.3 Hz aos 1 kHz com um ganho de 60 dB. Relativamente à linearidade, foi demonstrado que a relação entre o sinal de entrada (biopotencial) e o sinal à saída do TIA apresentam uma relação linear. Os testes realizados para confirmar o mínimo sinal detectado pela plataforma fotónica desenvolvida foram efectuados incluindo os estágios de filtragem e amplificação, resultando num ganho global de 4000 V/V. O sinal minimo detectável foi de 20 μV, a uma frequência de 10 Hz.

Por último, a plataforma desenvolvida foi testada em cenários reais na aquisição de diferentes biopotenciais – Electrocardiograma (ECG), Electroencefalograma (EEG) e Electromiograma (EMG). Os resultados obtidos foram comparados com plataformas convencionais nas mesmas condições. A plataforma fotónica apresentou boa capacidade para adquirir biopotenciais com conteúdo clinico relevante, assegurando a sensibilidade, resposta em frequência e remoção de artefactos desejável.

TABLE OF CONTENTS

LIST OF FIGURES

LIST OF TABLES

LIST OF SYMBOLS

Symbol	Description	Unit
A	Area of electrodes	m^2
A_{diff}	Differential gain	-
BW	Bandwidth	Hz
C	Cardiac equivalent vector	-
c	Speed of light	m/s
C_c	Virtual capacitor	F
C_C	Compensation capacitor	F
C_{cm}	Opamp common mode capacitance	F
C_{diff}	Opamp differential capacitance	F
C_{DL}	Double-layer capacitance	F
C_{eo}	Electro-optic modulator capacitance	F
C_{ep}	Epidermis capacitance	F
C_f	Transimpedance amplifier feedback capacitor	F
C_i	Transimpedance amplifier input capacitance	F
C_j	Photodiode junction capacitance	F
CNR	Carrier-to-noise Ratio	dB
CP	Carrier power	W
d	Electro-optic modulator electrode spacing	m
d_{eo}	Electro-optic crystal waveguide spacing	m
E	Electric-field	V/m
E_{hc}	Half-cell potential	V
f_c	Frequency of light	Hz
(f_{GBW}):	Opamp gain-bandwidth product	Hz
f_n	Filter natural frequency	Hz
f_{notch}	Notch frequency	Hz
f_p	High-frequency pole	Hz
G_{ph}	Photodiode gain	Hz
G_{TIA}	Transimpedance amplifier gain	V/A
h	Planck's constant	$J.s$
i_{bias}	Input bias current	A
i_D	Photodiode current source	A
i_{dark}	Photodiode dark current	A

IL	Insertion loss	dB
$i_{leakage}$	Photodiode leakage current	A
(i_{ph})	Photodiode output current	A
L	Electro-optic modulator electrode length	m
l	Electro-optic crystal waveguide length	m
L_{AB}	Lead between point A and B	m
V_{AB}	Potential difference between point A and B	V
v_{BIO}	Electrical potential of bioelectric signal	V
n	Refractive index of an electro-optic medium	-
n_e	Refractive index of the extraordinary ray of light	-
NEP	Noise equivalent power	$V / Hz^{1/2}$
NF_{ph}	Noise figure associated with the photodetector	dB
NF_{TIA} is the	Effective noise figure of the transimpedance amplifier	dB
n_0	Refractive index of the ordinary ray of light	-
q	electron charge	C
P_{in}	Input power of light	W
P_{out}	Modulated output power	-
R	Responsivity	A/W
R_C	Compensation resistor	Ω
R_{CT}	Double-layer resistance	Ω
R_{ep}	Epidermis resistance	Ω
R_f	Transimpedance amplifier feedback resistor	Ω
r_k	Kerr coefficient	m/V
RIN	Relative intensity noise	Hz^{-1}
r_p	Pockels coefficient	m/V
R_{sh}	Photodiode shunt resistance	Ω
R_{TIAeq}	Effective resistance load of the photodetector	Ω
R_s	Resistance associated with electrolyte	Ω
R_{ut}	Resistance associated with underlying tissue	Ω
s_{MZI}	modulation efficiency	W/V
T	Temperature	K
T_f	Transmission factor	-
v_{bias}	Bias voltage	V
V_{cm}	Common-mode potential	V
v_{in}	Input modulating voltage	V
V_{it}	Elecro-optic modulator total input voltage	V
$v_{maxtrans}$	Bias voltage at maximum transmission	V

V_{min}	Minimum detected voltage	V
$v_{mintrans}$	Bias voltage at minimum transmission	V
v_{out}	Transimpedance amplifier output voltage	V
v_{th}	Thermal voltage	V
v_+	Noninverting electrical potential at the input of the amplifier	V
v_-	Inverting electrical potential at the input of the amplifier	V
v_π	Half-wave voltage	V
w	Electro-optic crystal width	m
Z_t	Total impedance	Ω
Z_{in}	Input impedance	Ω
$\Delta\phi$	Phase variation	rad
ε_o	Medium permittivity	-
ε_r	Relative static permittivity	-
η	Quantum efficiency	-
λ	Wavelength	m
ϕ	Phase shift	rad
ω_H	High–pass cut-off frequency	rad/s
ω_L	Low–pass cut-off frequency	rad/s

LIST OF TERMS

Term	Designation
Ag	Silver
ASE	Amplified spontaneous emission
AV	Atrioventricular node
BCI	Brain-computer interface
CdTe	Cadmium telluride
Cl	Chloride
CMMR	Common-mode rejection ratio
CMOS	Complementary metal-oxide-semiconductor
CW	Continuous wave
EAP	Electroactive polymer
ECG	Electrocardiogram
ECoG	Electrocortigram
EEG	Electroencephalograms
EMG	Electromyogram
EO	Electro-optic
EOG	Electroocculogram
ENG	Electroneurogram
ERG	Electroretinogram
GTWM	Georgia Tech Wearable Motherboard
IC	Integrated circuit
InGaAs	Indium gallium arsenide
KD*P	Potassium dideuterium phosphate
LA	Left arm
LL	Left leg
LED	Light-emitting devices
$LiNbO_3$	Lithium niobate
$LiTaO_3$	Lithium tantalite
MM	Multimode

MRI	Magnetic resonance imaging
MZI	Mach-Zehnder interferometer
MU	Motor units
OE	Optoelectronic
OSA	Optical spectrum analyzer
PCB	Printed circuit board
PC-CLD-1	Polycarbonate with CDL-1 chromophore
PDA	Personal digital assistant
PIC	Photonic integrated circuit
PM	Polarization maintaining
PMMA-CDL1	Poly(methylmethacrylate) with CDL-1 chromophore
PVDF	Polyvinylidene fluoride
RA	Right arm
RF	Radiofrequency
SA	Sinoatrial node
Si	Silicium
SLED	Superluminescent light-emitting diode
SM	Single mode
SNR	Signal-to-noise ratio
TF	Transfer function
TIA	Transimpedance amplifier
UV	Ultraviolet
WHO	World Health Organization
ZnTe	Zinc telluride

Chapter 1

Introduction

Global expenditure on health care reached 10% of the gross domestic product in 2009 [1]. The development of continuous monitoring services could lead to significant savings in overall medical costs, since it would contribute to reduce hospitalization either through prevention of disease progress or by providing suitable resources for independent living [2].

Wearable technology represents a new emerging field with rising potential influence in several aspects of the modern healthcare sector, particularly in delivering point-of-care services. A wearable sensor is a comfortable and easy-to-use solution specifically designed with built-in electronic functions, for continuously monitoring an individual's health condition [3, 4]. These systems are valuable for many fields of applications (e.g. health monitoring, automotive and aeronautics) since they can provide levels of performance and capacities way ahead of the conventional systems. In addition, they also enhance the quality of life in patients in rehabilitation, chronically ill or disabled [4, 5].

1.1. Wearable Devices

Nowadays, quality of life is supported by medical resources that were not available in the past. The growing demand for wearable devices is being driven by the considerable need for a preventive medicine instead of reactive; the global increase of health awareness and also by the need of a proactive personal healthcare in a daily basis [6, 7].

A wearable medical device is as an unobtrusive, self-sufficient and ubiquitous system that supports continuous multi-parameter monitoring and treatment, and telemetric abilities [2, 3]. This contributes to a shift of health services from a conventional hospital-centered towards an individual-centered healthcare, which together with wireless technologies allows to a continuous feeding of relevant information back to the user and/or clinical professionals. In addition, they improve the early detection and timely response to possible health threats [2]. Since wearable, these devices are of portable nature and are sustained directly on the human body or in a part of clothing. Wearable monitoring devices sector is set to continue its rapid development throughout the years due to the added value brought to the healthcare market. According to a study made by ABI Research, the market for wearable devices will reach more than 100 million units per year, by 2016 [8].

The overall results of advances in both technological and healthcare sectors are leading to the establishment of a new paradigm – personalized health systems [2, 5]. These will enable the transfer of healthcare towards a system that will give the user a more pro-active role in its care, providing better monitoring and feedback with a comfortable and discreet solution. Likely to be a benefit to chronically ill and disabled, wearable health devices are an attractive solution for patients undergoing rehabilitation, providing them with independent living, since it allows to record and collect relevant data in the different situations of the individual's daily life [2, 3].

1.1.1 Applications

In wearable devices, a wide range of sensors is used to measure physiological and environmental conditions. The first type of sensors – physiological sensors – is used to monitor a clinical condition or process. Examples of signals measured with biomedical sensors are: heart, brain and muscle activity, blood pressure and body kinematics, among others. On the other hand, the second type of sensors – peripheral sensors – is responsible to sense the surrounding environmental conditions, enhancing the awareness of the

system [3, 9]. The diversity of wearable sensors and the trends in micro and nanofabrication will eventually lead to a widespread of applications for wearable devices.

Healthcare

Failure to do a more regular health monitoring condition can lead to problematic situations, specially considering the elderly with fragile and rapidly changing health status. In addition, Medical Doctors often cannot explain how most problems develop because they usually see the patients at a late stage of illness development [10]. According to the World Health Organization (WHO), in 2008, the number of deaths due to ischemic heart disease and from stroke or another form of cerebrovascular disease was 7.3 and 6.2 million, respectively [11]. Figure 1.1 shows the ten leading causes of death in 2008.

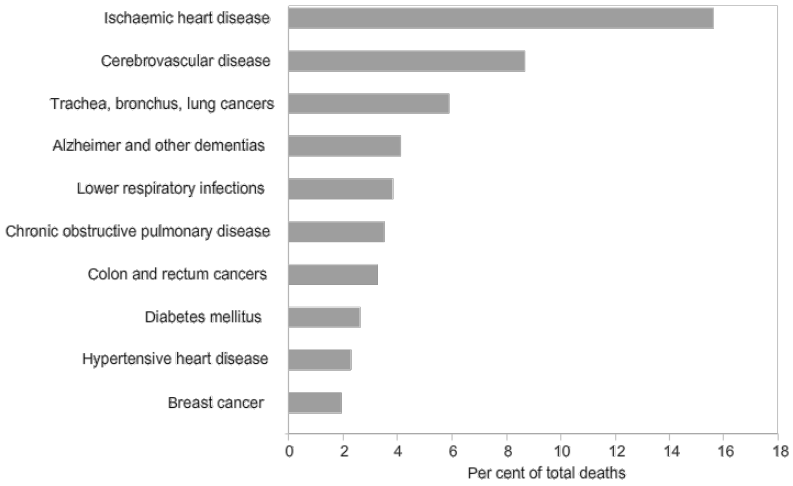

Figure 1.1 Ten leading causes of death in high-income countries in 2008 [10]. Data is taken over a sample population of 100000 inhabitants.

Regarding health conditions associated with circulatory and respiratory system, which represent the majority of deaths per year/100000 habitants (Figure 1.1), early and systematic intervention is highly valuable. The simultaneous and continuous recording of physiological signals allows to perform an intersignal elaboration and assessment of the patient's health condition status at any given time [10].

Many research groups have started to develop wearable technologies with main application in Health Science [12]. A valuable example of the importance of wearable devices in health monitoring and prevention can be found in a recent work developed by Kramer and co-workers [13]. They presented a wearable device for detecting seizures based on a three-axis accelerometer – "Motion Sensor". This device also has the ability to alert patients and families of possible seizures, as well as to assist in the preliminary recognition of these

events. Preliminary tests have suggested that this sensor/alarm correctly identified 91% of the seizures with a low false alarm rate. Another important example of the applicability of wearable sensors in improving health and quality of life, is the Brain Computer Interface (BCI). Wearable and wireless BCI systems are valuable in providing augmentation of human capabilities, useful in a wide spectrum of areas from health rehabilitation to virtual reality games. Several wearable BCI systems have been proposed in the past few years. A useful review of these devices can be found in [14].

Sports, Fashion and Leisure

Sports sector, that includes a broad range of modalities, is highly demanding since most activities (individual or in team) rely on extreme physical capacities. The constant and real-time monitoring of physiological signals, functional performance and activity of athletes is therefore of extreme importance, either during training or competition. Several studies have assessed the use of wearable sensors in recognition of activity for sports and daily activity applications [15, 16]. Both studies have indicated strong feasibility of wearable sensors for activity recognition in several conditions, which is valuable for promotion of health-enhancing physical activities and sport performance assessment.

Intelligent clothing and augmented reality is one of the most important applications of wearable devices in fashion and leisure [17]. Nowadays, well-known companies such as Philips and Infineon, have come with interactive clothing based on light-emitting devices (LEDs). Lumalive is an example of this technology composed of a photonic textile with lighted graphic display medium for text and animation [18].

Industrial and Military Applications

Industrial and military fields can benefit from wearable devices since they can assist either workers or soldiers in their functions, while providing real-time feedback on health status, context awareness and others. The European project PROETEX consists in the development of wearable prototypes for addressing Civil protection envisioning urban and forest fire fighters [19]. Another example related with military applications, is the work developed by Winterhalter et al. [20], which main goal is to develop textile-based wearable devices that can be integrated into military protective clothing.

1.1.2 Design Requirements

The design of wearable systems should follow a set of requirements, especially when compared to stationary equipment due to the various operating constraints. In fact, these solutions are often used in specific conditions and need to be integrated and functional into non-controlled environments where they will operate, e.g. exercise, sleep or work. In addition and particularly in health applications, the acceptability from behalf of patients and clinicians is crucial for the successful implementation of wearable devices [21].

A recent study called "Body-Worn Sensor Design: What Do Patients and Clinicians Want?" has a valuable review of some of the most important requisites regarding patients and clinician preferences [21]. From a user point a view, the main recurring factors were: less interference with daily life activities, compact, user-friendly, embedded technology, and reduce incomings to health care facilities. All of these issues are related with the esthetics of a wearable device [22]. On the other hand, clinicians are more concerned with technical issues such as long-term and real-time monitoring, attachment of the device to the patient and storage capacity. Figure 2.1 shows the key points that need to be covered along the wearable device creative process, divided in physical, user, performance and design-related requirements [3, 2, 23, 22].

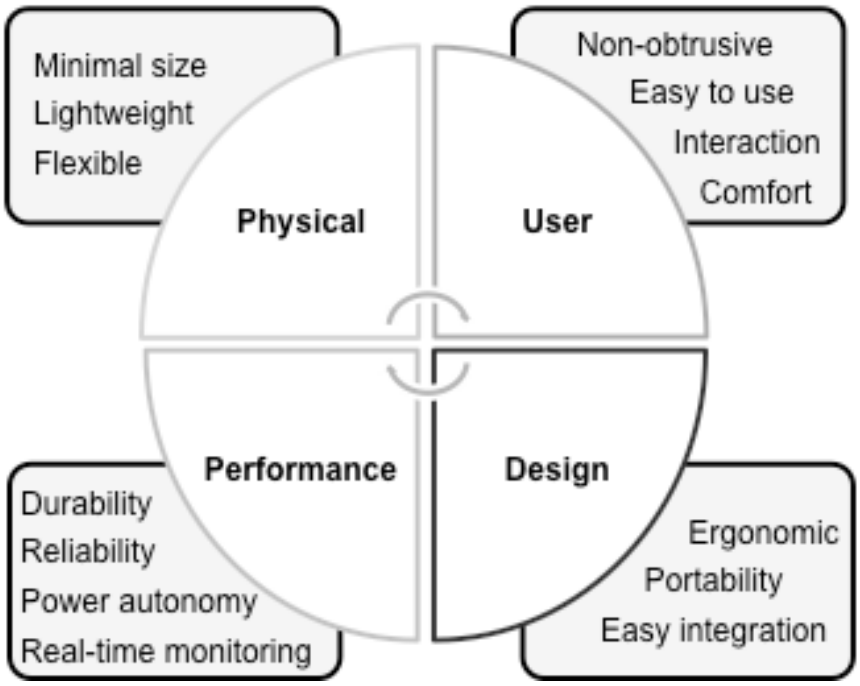

Figure 1.2 Main requirements for wearable devices acceptance by users and clinicians/technicians.

1.1.3 State of the Art

A number of wearable devices in the healthcare sector emerged in the past few years, ranging from simple monitoring of daily routine, to miniaturization and integration of sensors to enhance the overall performance of wearable systems. Wearable systems can be classified according to the level of integration of its components into the smart/functional material, i.e. substrate. There are three types of wearable systems according to this classification: 1st generation, based on attachable hardware components and sensors; 2nd generation, where these components are embedded into the material; and 3rd generation, where innovative integration techniques during the substrate material production allow for the design of multi-sensor clothing and/or accessories. Figure 1.3 presents the three generations of wearable systems, as well as some state-of-the-art for each category.

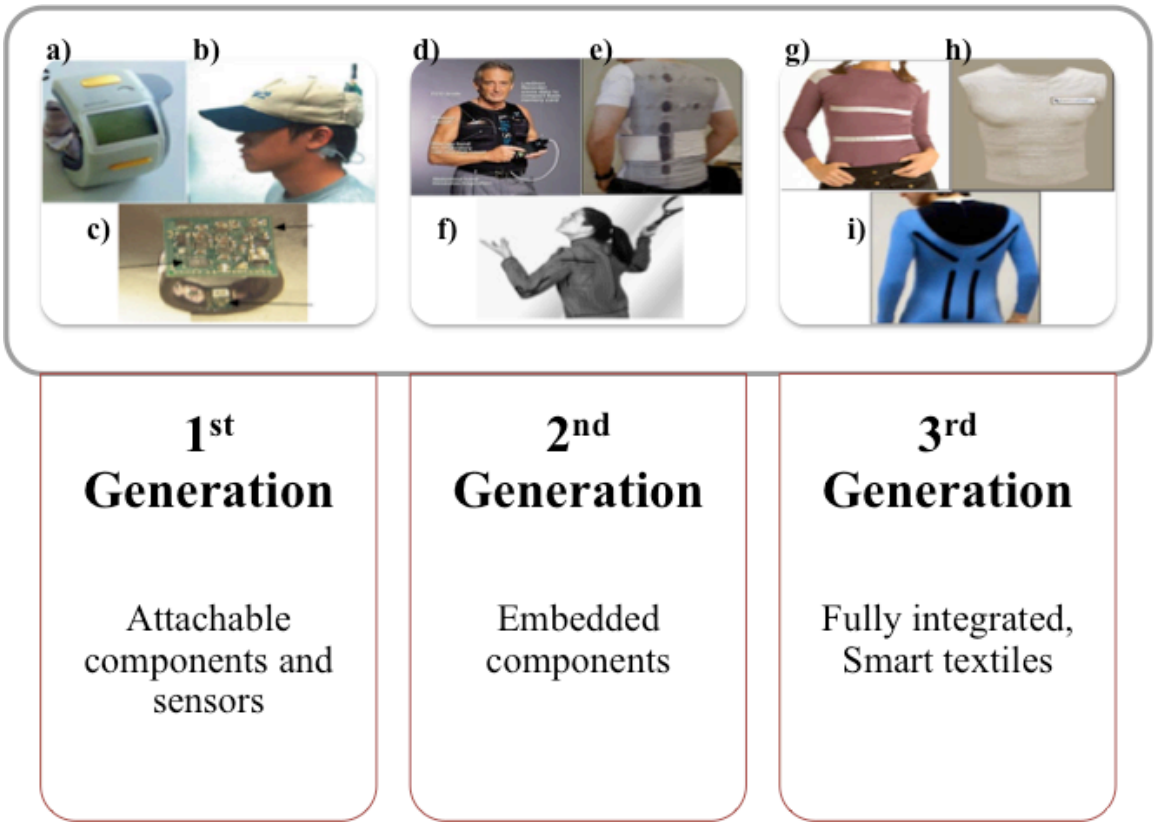

Figure 1.3 Categories of Wearable Devices and examples. Examples from the 1st generation of wearable devices from the left to the right are a a) wrist-worn device AMON [23], b) a braincap with a wireless Electroencephalography acquisition module [24] and c) a ring monitoring sensor [25]. The 2nd generation includes d) a monitoring t-shirt Lifeshirt [26], e) a sensorized T-shirt developed within the VTAM project [27] and f) a sensor jacket for context awareness [28]. The 3rd generation examples are g) a shirt developed by Smartex within the European integrated project WEALTHY [29], h) SmartShirt developed by Sensatex [21] and i) sensorized leotard developed [30].

The first wearable systems to appear were based on plug-in methods, where a supporting mechanism for attaching the necessary components is provided. These can include electrocardiogram (ECG) monitoring wristwatches, sensing components that can be attached to a t-shirt, a vest or even to a cap (Figure 1.3). The problem associated with these devices is its lack of comfort and practical solution considering the user's perspective. An example of the 1st category of wearable devices is described in the work entitled "AMON: A Wearable Medical Computer for High Risk Patients" [24]. The AMON system was developed by a European Union IST sponsored consortium and consists on a wrist worn unit with monitoring, data analysis and communication capabilities. This system is mainly intended for high-risk patients in need for constant monitoring. Choi and Jiang have developed a wearable sensor device in form of a belt-type sensor head, which is composed by conductive fabric and Polyvinylidene Fluoride (PVDF) film, for monitoring cardiorespiratory signals during sleep [25].

The drawbacks of the first generation of wearable systems leads to the design of a new generation based on partially embedded architecture, where all the necessary components are fixed to the substrate material. This not only eliminates the need for qualified personnel or for the user to place the components, running the risk of misplacement, but also allows for a more practical and discreet solution. However, there is still a considerable difference from a normal garment, meaning that the components have not a sufficient level of integration into the substrate, providing relatively comfortable solutions but yet perceptible. Lifeshirt is a product of Vivometrics, Inc. (Ventura, CA), and consists of a wearable physiological monitor in form of a chest and shoulder strap, providing non-invasive ambulatory monitoring of pulmonary cardiac function and posture [26].

The research and progress in integration techniques during the fabrication process leads to the design of a third generation of wearable health devices. This type of systems represents the front-end in wearable technology allowing to design smart, functional and multi-sensing materials that, due to the high level of integration, are apparently normal. A very popular technological example of a 3rd generation wearable system is the electronic textile – e-textile – which consists of high knowledge-content garments provided by multifunctional fabrics. Through blending of components into the user's ordinary clothing, it is possible to achieve an ideal wearable system, minimizing the hassle of wearing the device. The Georgia Institute of Technology (Atlanta) jointly with the U.S. Navy proposed one of the first wearable solutions, which consisted of a wearable vest embedded with optical fibers and sensors, working also as a data bus – the Georgia Tech Wearable Motherboard (GTWM) [27]. All the components are integrated into the fabric creating a flexible device, which was manufactured essentially for

use in combat conditions. This device was placed into the market by Sensatex, Inc., as a product named SensatexSmart Shirt. The paper "Advances in textile technologies for unobtrusive monitoring of vital parameters and movements" describes the project called MyHeart that consists in functional clothes with on-body sensors and electronics to acquire, process and evaluate physiological data [28].

1.1.4 Integration

Wearable devices should consist on elegant, easy to wear and ubiquitous clothing in order to accompany the user to any place at any time. This requires the integration of sensors/actuators, power sources, processing and communication functions within the wearable material [4, 23]. First, researchers have explored the use of plug-in modules and attachable off-the-shelf electrical and optical devices and components. Nevertheless, is unsuitable for lengthy continuous monitoring due to the cumbersome modules to be carried out by the user. These limitations can be addressed with an integration of multiple smart functions into textiles or other materials.

Textiles are an ideal substrate for integrating miniaturized components since they are comfortable, pervasive and constitute the basis of almost every piece of cloth. The implementation of wearable sensors towards completely flexible devices can be performed in two major ways: the sensors can be embedded in the textile; or the fabric itself is used as a sensing structure or suite. The first approach implies the use of interconnections based on electro-active fibers, either metallic or optical, whereas the latter method consists in developing conductive yarns and fabrics with sensing capabilities [9, 29].

The use of purely electrical approaches implies the problem of local power supply and complex interconnections within the wearable suit. On the other hand, with optical fiber sensors, it's possible to design all-optic suits with attachable power supply units, in a plug-in module such as a belt. This opens the opportunity to use these devices in conditions where electrical system leans to fail, such as electromagnetic rooms (MRI rooms), or other harsh conditions [30, 31]. Many approaches to optical fibers integration have been developed, with particular interest for wearable health devices, leading to easier optical fiber integration into textiles and other wearable materials [32-36]. Since textiles are composed by a combination of multiple yarns and fibers with resemblance to optical fibers, integration of these sensors into the textile is easy and without making the final product locally thicker [30, 37]. This is possible due to the compatibility between optical and textile fibers in terms of fineness and thickness. Looking into more detail into optical fiber properties, these components have

tensile strengths about 10 to 100 times larger when compared to textile fibers, resulting in more resistance to tensile load [30]. Common fabric manufacturing processes can be used to integrate optical fibers into textiles, such as weaving, knitting and spread-coating. The latter technique is one of the most promising ones since it allows to reach higher degrees of process flexibility is spread-coating which consists in producing a sandwich structure of laminates with different materials [37]. Due to it's nature of layer by layer, spread coating guarantees high-process flexibility, use of different materials and geometries, and reliable fiber positioning.

1.2 Wearable Photonic Systems

Research in photonics began between 1960s and 1970s, when lasers and light emission through optical fibers were introduced. This field is particularly profitable in applications where conventional electronic interconnections meet inherent restrictions caused by attenuation, power consumption and crosstalk. As a result, photonic sensors have become increasingly used in several fields of applications such as Healthcare, Military, Industrial or Sports. This technology-based sensors have demonstrated great capabilities as candidates for monitoring physiological and environmental changes and they offer many advantages, such as [36, 39, 44, 45]:

- Easy integration into a widespread of materials and structures;
- Resistance to harsh environments and to corrosion;
- Immunity to electromagnetic and radio frequency interference;
- Multiplexing capacity towards the design of sensing networks;
- Remote and multifunctional sensing capability;
- Electrical wire free;
- Small size and lightweight;
- Long lifetime (more than 25 years).

In addition, photonic sensors have a great economic impact considering that the global market for biophotonics is forecasted at $133 billion by 2016, with a yearly growth rate of 31% [38].

1.2.1 Bioelectric Signal Photonic Sensing

Physiological signals include bioelectric events and other biochemical and physical parameters that are crucial for assessment of the user's health status. In particular, bioelectric signals represent the electrical activity related to the physiology and function of organs and systems, such as heart, brain and muscles [22, 23].

Bioelectric signals can be detected in suitable sites on the surface of the body, since the electric field propagates through the biological medium. Therefore, this allows for a non-invasive acquisition of such signals providing vital clues as to normal functions of organs. This leads to useful and reliable means of health condition monitoring. For example, Electroencephalograms (EEG), a bioelectric signal originated by brain activity, can help to identify epileptic seizure events [13, 39].

Not every sensor can be used in a wearable context, specially looking at the user's perspective. It has to be taken into account not only its physical attributes such as size and weight, but also its non-invasive character and easy placement. In addition, these sensors must ideally produce an electrical output in order to be digitally processed, being durable, reliable and low-power consumption [3, 40].

Photonic sensors fulfill the above requirements with the added value of eliminating the use of electrical connections in the piece of cloth or accessories. When dealing with photonic sensors, the following main function blocks are needed to correctly perform bioelectric sensing: optical signal generation, light modulation and photodetection. Figure 1.4 shows the typical acquisition system of an optical sensor.

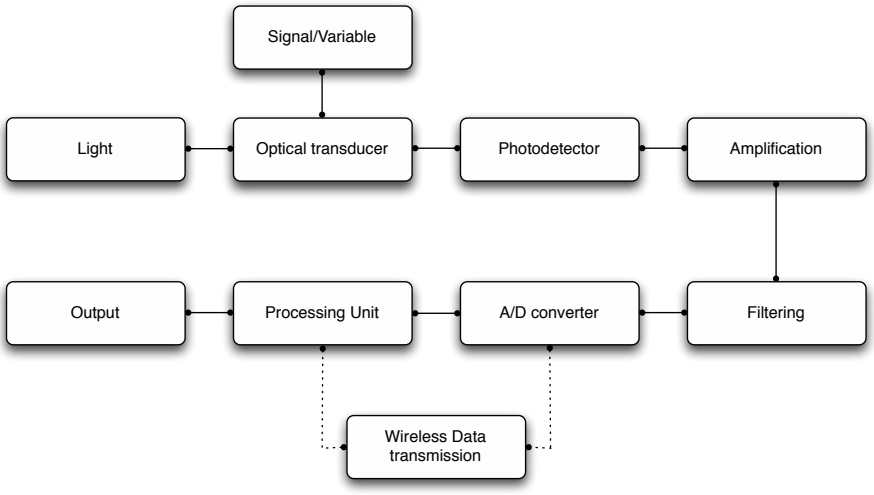

Figure 1.4 Optical sensor acquisition block diagram.

Photonic acquisition systems must include a light source that will pass through an optical transducer, i.e. optical modulator. In the presence of a particular signal, the optical

transducer will produce a shift in light properties, whether if it's intensity, phase, polarization or other. Afterwards, a photodetector is responsible to collect this modulated light, converting this optical modification into a electrical entity. The latter is dependent on the type of photodetection circuitry applied in this stage, where a photodiode can be used in order to convert light intensity into current or voltage. The analog signal obtained is converted to digital forms by A/D converters and further processed using different algorithms. If necessary the processed signals can be converted back to analog forms to drive specific devices. Some applications, it's often necessary to include wireless communication systems that enable the sensing component to transmit the data to a control-processing unit or even to a database service.

1.2.2 EO Sensing Methodologies

Electro-optic (EO) sensors use specific transducer effects by which an optical signal or material exhibits a particular response in the presence of an external electric field. The materials exhibiting this type of stimulus-response mechanism are classified as EO materials. Some of these materials are included in Table 1.1. The EO component works as the sensing element, which can be in form of a coating material, such as a hydrogel or a piezoelectric material, or even used as a device like an EO intensity modulator. Several effects or materials can be used as the EO sensing component, and they can be divided into different categories, each of one with a specific associated effect. Table 1.1 shows some of the different effects that can be applied in the sensing mechanism of a photonic wearable device, as well as examples of materials and signals detected.

Table 1.1 Different EO transducer effects applied in the sensing mechanism for wearable devices [29, 41-43].

Transducer Effect	Sensing devices	Stimulus	Response	Examples of Materials	Bioelectric signal
Electro-optic	EO modulators	Electric field	Birefringence	Lithium Niobate ($LiNbO_3$), Lithium tantalite ($LiTaO_3$), EO polymers	EEG, ECG, EMG, EOG
Electroluminescence	Light Emission Devices	Electric field	Light emission	Electroactive Polymers (EAPs)	ECG, EMG
Photoluminescence	Photoluminescense sensors Example: UV radiation sensor	Incident light	Light emission		UV radiation

Since the stimulus for EO operation relies on an external electric field, an important feature of photonic sensors is the ability to more easily enable contactless measurements of physiological events, particularly electrophysiological signals.

1.2.3 Bioelectroptic Sensing – State of the Art

A few studies have explored the use of EO sensors in wearable monitoring bioelectric activity [44, 45]. In particular, Kingsley and co-workers, have developed an EO sensor based on intensity modulation called Photrodes™. This sensor is specially envisioned for EEG and ECG monitoring of Army soldiers [46]. Despite proper operation, these works are not a complete photonic bioelectric sensing platform.

1.3 Motivation and Objective

Current healthcare systems are facing a fundamental transformation mainly driven by the growing aging population, increasing healthcare costs, reduced quality of life and prevalence of chronic diseases. People are acquiring more health consciousness and are prone to assume a more active role in managing their own health and life style [6].

The development of miniature and portable sensors that can be used unobtrusively or can be part of clothing items, i.e., wearable sensors, have opened countless solutions to deliver healthcare beyond the hospital context, in the home or during outdoor daily activities. These systems enhance the quality of life of patients in rehabilitation, chronically ill or disabled, while being financially rewarding by reducing hospitalization. In fact, this can be achieved either through prevention of disease progress or by providing suitable resources for independent living [3].

Regardless of other physiological signals, bioelectric monitoring is of extreme importance, since it provides information on the activity of organs such as heart, brain, and muscles. Such information is required not only when assessing and monitoring patient's health status, but also valuable under non-clinical scenarios, such as for monitoring professional workers, particularly when in contact with stressful conditions. Therefore, the development of sensing interfaces designed to non-invasively obtain the ECG, EMG and EEG is demanded.

Despite the ability to monitor the low-amplitude high-impedance bioelectric signals sources, available technologies have not yet solved the drawbacks associated with embedding sensors and electronic components into clothing items. The most advanced wearable solutions are based on conductive fabrics that use conductive fibers or yarns, serving as interconnects and sensors [29, 37]. Nevertheless, since using electrical interconnections, such technologies are highly susceptible to electromagnetic interferences and movement artifacts. Moreover, such solutions require the use of probe currents or voltages that may raise safety concerns.

Photonic technologies contribute to the development of sensing solutions when electrical counterparts fail due to problems associated with power consumption, power loss, or electromagnetic interference. Features such as miniaturization, flexibility, multiplexing capabilities and the fact that transmission losses of optical signals are considerably reduced, underscore their great promise. Photonic sensors show compact design and high level of integration into several materials, whereas the problem with interconnections and electronics is considerably reduced [32-36]. The embedment of photonic sensing elements into clothing items makes possible to achieve long-term monitoring of multi-parameter, while being easily customized according to the needs of each individual system, promoting the comfort when wearing such systems. In fact, recent integration technologies have proven to be feasible for optical fiber integration into polymeric materials [34]. Recent studies have also explored optical-based sensors for bioelectric activity recording [44, 45] but, despite the obtained good results, a full solution to acquire the main bioelectric signals, i.e. ECG, EMG and EEG is still lacking.

The main achievement of this thesis was the design and characterization of a multi-bioelectric signal acquisition platform, based on photonic technologies, suitable for further use in wearable applications. The system investigated in this thesis is based on electro-optic (EO) methods, consisting in a Lithium Niobate ($LiNbO_3$) Mach-Zehnder Interferometer (MZI) modulator, and optoelectronic (OE) circuitry for signal translation, filtering and amplification (Figure 1.5). The designed platform allows for multiple bioelectric signals to be extracted and recorded from several locations, and the front-end acquisition is only composed by optical fibers as interconnections. The main goal is to provide a photonic platform compatible with integrated and miniaturized components towards the design of wearable monitoring garment. This garment could include, for instance, a wearable brain cap for EEG monitoring and a t-shirt or vest for ECG and EMG monitoring.

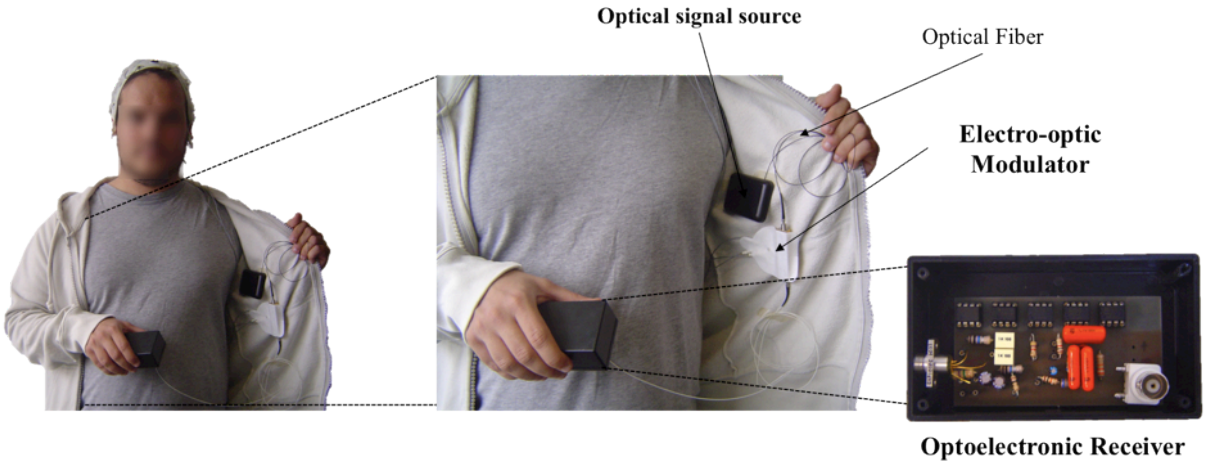

Figure 1.5 Photonic platform for bioelectric signal acquisition on wearable devices, developed in this thesis.

1.4 Thesis Organization

This chapter introduced the subject of wearable devices in healthcare and presented the thesis's motivation as well as the objectives. Chapter 2 describes the bioelectric signal acquisition theory, including its signal properties as well as typical acquisition components. Chapter 3 focuses on the photonic bioelectric signal sensor, particularly in the phenomena behind the sensor mechanism and the selected components. Technology selection is explored and analyzed in terms of performance and modeled in order to determine the bottleneck of the photonic system. Chapter 4 deals with the OE system design that supports the EO conversion performed during bioelectric signal acquisition. The performance of the OE system is analyzed following Chapter 3 system overview. Chapter 5 presents the developed prototyped for testing photonic bioelectric signal acquisition and results. These results consisted in first analyze overall photonic platform bioelectric acquisition in terms of sensitivity, process linearity throughout EO and OE stages. Additionally, the developed photonic platform is compared with standard bioelectric acquisition setups using human subjects. Finally, Chapter 6 draws the main conclusions as well as a few recommendations for future work.

References

[1] WHO, "http://www.who.int/gho/health_financing/en/index.html," 2011.

[2] X.-F. Teng, Y.-T. Zhang, C. C. Y. Poon, and P. Bonato, "Wearable Medical Systems for p-Health," *Biomedical Engineering, IEEE Reviews in*, vol. 1, pp. 62-74, 2008.

[3] D. I. Fotiadis, C. Glaros, and A. Likas, "Wearable Medical Devices," in *Wiley Encyclopedia of Biomedical Engineering*, John Wiley & Sons, Inc., 2006.

[4] P. Lukowicz, T. Kirstein, and G. Tröster, "Wearable systems for health care applications.," *Methods of information in medicine*, vol. 43, no. 3, pp. 232-8, Jan. 2004.

[5] S. Park and S. Jayaraman, "Enhancing the quality of life through wearable technology.," *IEEE engineering in medicine and biology magazine : the quarterly magazine of the Engineering in Medicine & Biology Society*, vol. 22, no. 3, pp. 41-8, 2003.

[6] A. Lymberis, "Intelligent biomedical clothing for personal health and disease management: state of the art and future vision," *Telemedicine Journal and e-health*, vol. 9, no. 4, 2003.

[7] J. E. Bardram, "Pervasive Healthcare as a Scientific Discipline," *Methods of Information in Medicine*, pp. 178-185, 2008.

[8] A. Bonfiglio, *Wearable Monitoring Systems*. Springer Verlag, 2010.

[9] P. Bonato, "Clinical applications of wearable technology.," *Conference proceedings : ... Annual International Conference of the IEEE Engineering in Medicine and Biology Society. IEEE Engineering in Medicine and Biology Society. Conference*, vol. 2009, pp. 6580-3, Jan. 2009.

[10] WHO, "http://www.who.int/whosis/whostat/2011/en/index.html," 2011. [Online]. Available: http://www.who.int/whosis/whostat/en/index.html.

[11] A. Pantelopoulos and N. G. Bourbakis, "A Survey on Wearable Sensor-Based Systems for Health Monitoring and Prognosis," *IEEE Transactions on Systems, Man, and Cybernetics, Part C (Applications and Reviews)*, vol. 40, no. 1, pp. 1-12, Jan. 2010.

[12] U. Kramer, S. Kipervasser, A. Shlitner, and R. Kuzniecky, "A Novel Portable Seizure Detection Alarm System: Preliminary Results," *Journal of Clinical Neurophysiology*, vol. 28, no. 1, p. 36, 2011.

[13] C.T. Lin et al., "Review of wireless and wearable electroencephalogram systems and brain-computer interfaces--a mini-review.," *Gerontology*, vol. 56, no. 1, pp. 112-9, Jan. 2010.

[14] M. Ermes, J. Pärkka, J. Mantyjarvi, and I. Korhonen, "Detection of daily activities and sports with wearable sensors in controlled and uncontrolled conditions.," *IEEE transactions on information technology in biomedicine : a publication of the IEEE Engineering in Medicine and Biology Society*, vol. 12, no. 1, pp. 20-6, Jan. 2008.

[15] J. Pärkkä, M. Ermes, P. Korpipää, J. Mäntyjärvi, J. Peltola, and I. Korhonen, *Activity classification using realistic data from wearable sensors.*, vol. 10, no. 1. Piscataway, NJ: IEEE, c1997-, 2006, pp. 119-128.

[16] T. Starner, S. Mann, B. Rhodes, and J. Levine, "Augmented reality through wearable computing," *Presence:*, 1997.

[17] Philips, "Philips Lumalive fabrics – creating a magic lighting experience with textiles "," *World*, no. 28, 2006.

[18] D. Curone et al., "Smart garments for safety improvement of emergency/disaster operators.," *Conference Proceedings of the International Conference of IEEE Engineering in Medicine and Biology Society*, vol. 2007, pp. 3962-3965, 2007.

[19] C. A. Winterhalter et al., "Development of electronic textiles to support networks, communications, and medical applications in future U.S. military protective clothing systems.," *IEEE transactions on information technology in biomedicine a publication of the IEEE Engineering in Medicine and Biology Society*, vol. 9, no. 3. pp. 402-406, 2005.

[20] J. H. M. Bergmann and a H. McGregor, "Body-worn sensor design: what do patients and clinicians want?," *Annals of biomedical engineering*, vol. 39, no. 9, pp. 2299-312, Sep. 2011.

[21] F. Gemperle, C. Kasabach, J. Stivoric, M. Bauer, and R. Martin, "Design for wearability," *Digest of Papers. Second International Symposium on Wearable Computers (Cat. No.98EX215)*, pp. 116-122.

[22] S. Park and S. Jayaraman, "Smart textiles: Wearable electronic systems," *MRS bulletin*, vol. 28, no. 8, pp. 585–591, 2003.

[23] U. Anliker et al., "AMON: a wearable multiparameter medical monitoring and alert system," *Ieee Transactions On Information Technology In Biomedicine*, vol. 8, no. 4, pp. 415-427, 2004.

[24] S. Choi and Z. Jiang, "A novel wearable sensor device with conductive fabric and PVDF film for monitoring cardiorespiratory signals," *Sensors and Actuators A: Physical*, vol. 128, no. 2, pp. 317-326, Apr. 2006.

[25] P. Grossman, "The LifeShirt: a multi-function ambulatory system monitoring health, disease, and medical intervention in the real world.," *Studies In Health Technology And Informatics*, vol. 108, pp. 133-141, 2004.

[26] C. Gopalsamy, S. Park, R. Rajamanickam, and S. Jayaraman, "The Wearable MotherboardTM : The First Generation Responsive Textile Structures Medical Applications," *Virtual Reality*, pp. 152-168, 1999.

[27] R. Paradiso and D. De Rossi, "Advances in textile technologies for unobtrusive monitoring of vital parameters and movements.," *Conference proceedings : ... Annual International Conference of the IEEE Engineering in Medicine and Biology Society. IEEE Engineering in Medicine and Biology Society. Conference*, vol. 1, pp. 392-5, Jan. 2006.

[28] F. Carpi and D. De Rossi, "Electroactive polymer-based devices for e-textiles in biomedicine," *Information Technology in Biomedicine, IEEE Transactions on*, vol. 9, no. 3, pp. 295–318, 2005.

[29] J. Rantala, J. Hännikäinen, and J. Vanhala, "Fiber optic sensors for wearable applications," *Personal and Ubiquitous Computing*, vol. 15, no. 1, pp. 85-96, Jun. 2010.

[30] J. Hesse and W. Sohler, "Fiber optic sensors," *Oceans 82*, no. 1, pp. 257-259, 1984.

[31] F. Berghmans et al., "Photonic Skins for Optical Sensing Highlights of the PHOSFOS Project," *20th International Conference on Optical Fibre Sensors, Proceedings of the SPIE, vol. 7503, pp. 75030B-75030B-*, vol. 4, 2009.

[32] M. a El-Sherif, J. Yuan, and A. Macdiarmid, "Fiber Optic Sensors and Smart Fabrics," *Journal of Intelligent Material Systems and Structures*, vol. 11, no. 5, pp. 407-414, May. 2000.

[33] A. Ferreira et al., "A Smart Skin PVC Foil Based on FBG Sensors for Monitoring Strain and Temperature," no. c, 2010.

[34] E. Bosman et al., "Fully Flexible Optoelectronic Foil," *IEEE Journal of Selected Topics in Quantum Electronics*, vol. 16, no. 5, pp. 1355-1362, Sep. 2010.

[35] E. Bosman, G. Van Steenberge, P. Geerinck, J. Vanfleteren, and P. Van Daele, "Fully embedded optical and electrical interconnections in flexible foils," in *Microelectronics and Packaging Conference, 2009. EMPC 2009. European*, 2009, pp. 1–5.

[36] X. Tao and T. Institute, *Wearable electronics and photonics*. Crc Press, 2005.

[37] "Biophotonics Market Predicted to Hit $133 Billion by 2016." [Online]. Available: http://www.photonics.com/Article.aspx?AID=27453.

[38] N. Verma, A. Shoeb, J. Bohorquez, J. Dawson, J. Guttag, and A. P. Chandrakasan, "A Micro-Power EEG Acquisition SoC With Integrated Feature Extraction Processor for a Chronic Seizure Detection System," *IEEE Journal of Solid-State Circuits*, vol. 45, no. 4, pp. 804-816, Apr. 2010.

[39] J. M. Winters, Y. Wang, and J. M. Winters, "Wearable sensors and telerehabilitation.," *IEEE engineering in medicine and biology magazine : the quarterly magazine of the Engineering in Medicine & Biology Society*, vol. 22, no. 3, pp. 56-65, 2003.

[40] G. K. Knopf and A. S. Bassi, *Smart biosensor technology*. CRC Press, 2007, p. 636.

[41] R. Lane and B. Craig, "Materials that sense and respond – An introduction to smart materials," *Structure*, vol. 7, no. 2, pp. 9-14.

[42] J. Luprano, J. Sola, A. Ridolfi, S. Pasche, and B. Gros, "New generation of smart sensors for biochemical and bioelectrical applications," *Strain*, 2007.

[43] S. a Kingsley, "Photrodes for physiological sensing," *Proceedings of SPIE*, pp. 158-166, 2004.

[44] A. Sasaki, A. Furuya, and M. Shinagawa, "Study of semiconductor electro-optic modulators for sensing extremely-low-frequency electrical signals," *Sensors and Actuators A: Physical*, vol. 151, no. 1, pp. 1-8, Apr. 2009.

[45] S. A. Kingsley, "Revolutionary optical sensor for physiological monitoring in the battlefield," *Proceedings of SPIE*, vol. 5403, pp. 68-77, 2004.

Chapter 2

Wearable Bioelectric Signal Acquisition

Bioelectric signals or biopotentials are generated by nerves and muscles and embody the activity of particular organs: the heart, brain and muscle [1, 2]. The continuous acquisition of these physiological signals allows to detect and prevent the progress of certain diseases such as cardiovascular diseases or neurological pathologies. In addition, it also has the potential to support the rehabilitating and chronic ill patients. Bioelectric signals are obtained through specific electrodes that establish an interface between the human body and the measurement apparatus [3]. In order to design readout circuits to measure bioelectric signals and to provide solutions for real-time monitoring, it's necessary to cope with various problems due to particular characteristics of these signals, as well as with environmental and device-related interferences. Therefore, the design of wearable bioelectric acquisition systems

requires a solid understanding of the origin and characteristics of bioelectric signals as well as the system components and design.

This chapter will focus on introducing the origin and principle of bioelectric activity as well as the measurements and acquisition system involved particularly in detecting the electrocardiogram (ECG), the electroencephalogram (EEG), the electromyogram (EMG), and the electrooculogram (EOG).

2.1 Bioelectric Signals

In order to fully understand the nature and characteristics of bioelectric signals it's necessary to explain the basics of bioelectricity phenomena and how these signals are originated. There are different types of bioelectric signals, depending on the organ or function they are associated with. All these points are explained in detail further along this chapter.

2.1.1 Origin

Bioelectricity is a phenomenon existent in many living element (cells, tissues, organs) and provide both steady and time-varying electric potentials that represent certain functions of organs such as heart, brain and muscles. Biological tissues can be considered as electric volume conductors, supporting the conduction of currents [4]. On a larger scale, few places in the body are non-conductors, which reflect the little amplitude variance occurred from one part of the body to another. Therefore any current generator within the body can create electric fields that can be acquired from most parts of the human skin, usually called bioelectric signals [1].

Bioelectric processes occur at the cellular level resulting in segregation of charge and thereby electric fields within the body. These cells are called excitable cells and when stimulated they undergo depolarization, giving origin to action potentials . The occurrence of this phenomenon is accompanied by physiological events such as transmission of information along nerve cells or the contraction of cardiac cells [1, 5]. Figure 2.1 shows the action potential generation mechanism along with the structure of a cell membrane.

A single excitable cell exhibits a resting potential of around 70mV with respect to the extracellular medium [1, 4]. At this state, the membrane of the cell is more permeable to K^+ than Na^+, with higher intracellular concentrations of K^+. The transport of these ions is made through cell molecular pumps and selective ion channels (Figure 2.1).

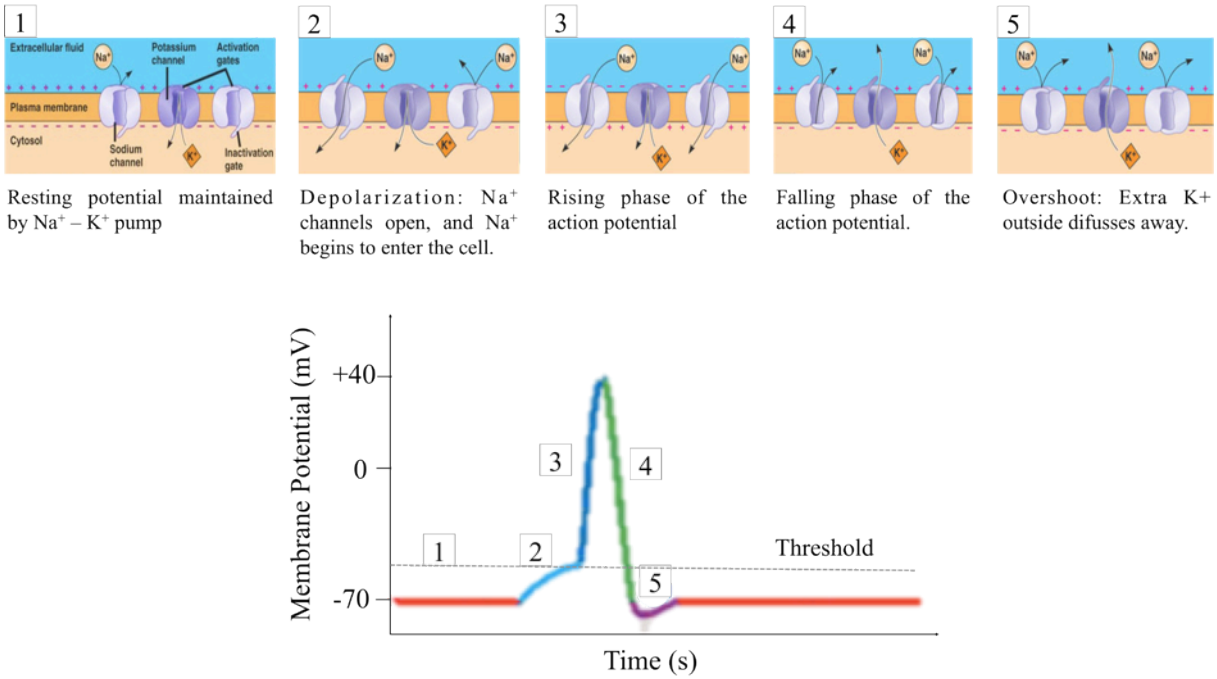

Figure 2.1 Action potential generation mechanism. Each step is represented in the action potential plot, as a colored region.

When a cell is electrically stimulated and exceeds a certain threshold value (typically of 20 mV), the membrane potential starts a rapid depolarization due to a change in permeability towards the increase in Na^+ ions. This causes the Na^+ ions to diffuse inwards the cell and results in a potential increase in the interior of the cell. When the potential reaches a value close to 40 mV, the Na^+ ion permeability starts to increase more slowly, allowing the ions to flow from inside to outside, returning the membrane potential to its resting value [1, 2, 4].

An action potential corresponds to this cycle of cellular potential (Figure 2.1), and resultant generated currents propagate themselves giving origin to bioelectric signals, such as ECG, EEG, EMG and EOG [1, 5].

2.1.2 Main Bioelectric Signals

Each excitable cell produces a characteristic action potential, that depending on propagation and location, giving rise to different bioelectric signals. For example, the activity of cells of a massive number of neurons results in EEG signal, activity of cells in the sinoatrial node of the heart produces an excitation that when propagated throughout the heart results in ECG. Thus, it is clear that depending on the type of cell, different bioelectric signals are produced, with distinct characteristics and measurement procedures [4].

Despite the existence of more bioelectric signals, ECG, EEG, EMG and EOG are the most important considering a wearable monitoring context. In addition, the detection of these bioelectric signals is performed non-invasively, i.e. on the surface of the skin.

ECG

The first findings of heart bioelectrical phenomena occurred back in 1842, when Calo Matteucci (Italian physicist) found that each heartbeat is accompanied by an electric current [6]. Since then, a lot of effort has been put into ECG research. An ECG is a recording of bioelectric signals originated from cardiac electric activity, usually measured by placing electrodes directly on the body [7]. This activity is known to reflect the activity of the heart muscle underneath and in its proximities.

The heart comprises four types of tissues: sinoatrial node (SA) and atrioventricular node (AV), atrial, Purkinje, and ventricular tissue. These tissues are composed of excitable cells exhibiting its own characteristic action potential [1, 7]. Figure 2.2 depicts the heart anatomy and the bioelectric events occurred during an ECG.

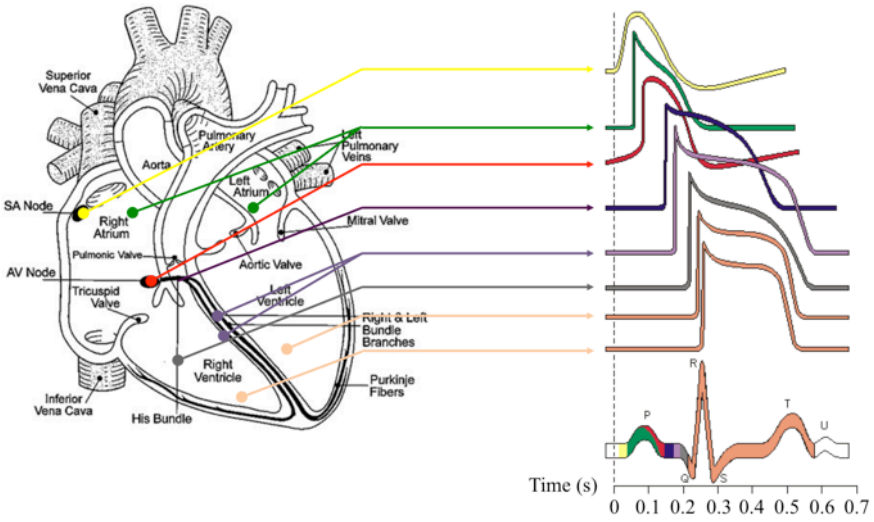

Figure 2.2 Heart anatomy and major bioelectric events of a typical ECG.

Cardiac electric activity starts at the SA node and is then conducted to the ventricles. The complete ECG is shown in Figure 2.2 and it can be divided in three components, each one corresponding to a specific electrical activity phenomena: P wave, QRS complex and T and U waves. The P wave corresponds to activation or depolarization of the atrial cells, arising from the SA node. Following this wave, an isoelectric segment (P-R segment) appears preceding a rapid and large deflection that corresponds to the excitation of ventricles – QRS complex. This complex begins with a descending deflection, the Q wave, headed by R wave (upward deflection) and ending with a downward deflection, the S wave. Finally, ventricles

return to their electrical resting state showing a low-frequency T and U waves that indicate the ventricular repolarization. This series of bioelectric events form a cardiac cycle, i.e. heartbeat, and being the normal heart rate comprised in the range of 60 to 100 beats per minute. Common abnormalities detected in ECG are identified through the analysis of these waveform components and examples are: absence of P waves, fast or slow heart rates and non isoelectric ST segments [1, 7, 8].

Physically, the simplest model for linking the cardiac generator to the body surface potentials and provide a framework for the study of clinical ECG is the dipole model. Therefore, heart's activation is an electric vector usually called cardiac equivalent vector (*C*), which can be measured if using a differential recording [9]. Basically, two electrodes are placed on the body forming a lead (L_{AB}) between them, and the potential difference between them, measured on the surface is:

$$V_{AB}(t) = C(t) \bullet L_{AB}(t), \tag{2.1}$$

where A and B represent both measurement locations. This concept of leads was first introduced by Willem Einthoven in 1902, when he proposed a measurement convention named after him – Einthoven lead system [10]. The approach comprises a combination of electrodes taking measurements from different leads: limb and chest leads. Figure 2.3 translates the Einthoven's assumption that the heart is the electric center of a triangle defined by the leads – the Einthoven triangle [7].

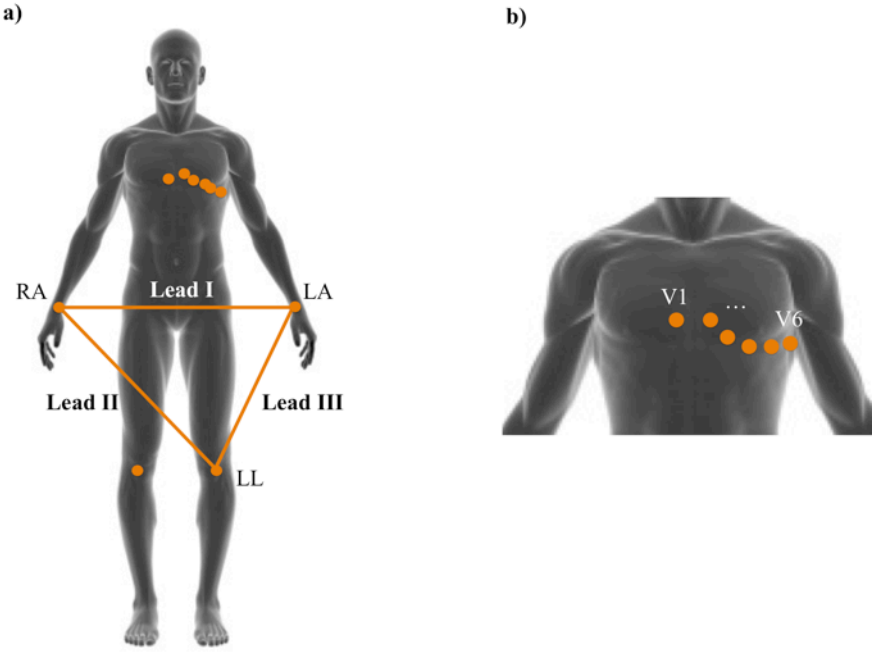

Figure 2.3 Einthoven lead system: a) limb leads, and b) chest leads (leads are incrementally numerated from V1 to V6.

According to this methodology, an ECG is obtained through the derivation of three limb electrodes, i.e. leads, and their potentials are called lead I, II and III. Each one of these leads is defined as:

$$I = V_{LA} - V_{RA} \tag{2.2}$$

$$II = V_{LL} - V_{RA} \tag{2.3}$$

$$III = V_{LL} - V_{LA} \tag{2.4}$$

where subscript RA = right arm, LA = left arm, and LL = left leg. Einthoven's leads fulfill an electrical outlook of the heart from three different vectorial directions. In addition to these limbs, unipolar leads aVR, aVL and aVF can be used to record the potential at the electrode placed in the right arm, left arm and left foot, respectively. The remaining six leads V1, V2, V3, V4, V5 and V6 are designated as chest leads and together with the other leads contribute to define the nature and status of the activity on a specific part of the heart muscle. For instance, inferior myocardial infarction produces main changes in the leads that explore the heart from below, i.e. leads II, III and aVF. At ECG frequencies (0.05 – 150 Hz), the human body is assumed as merely resistive, allowing to consider the four limbs as wires attached to the torso. Therefore it's possible to record a lead in different locations of the limb, without loss of cardiac information. Nevertheless, there is a signal magnitude variation that is induced by different inter-electrode distances and locations [7].

In a study performed by Merja Puurtine and co-workers it was shown that ECG amplitude is affected by the inter-space electrode distance. For instance, the recorded amplitude for the electrode pair V2–V6 and V1–V2 were, respectively, 3.711 mV and 1.401 mV [11]. Therefore, higher amplitudes are obtained with longer inter-electrode spacing. Despite this, there is a point where the distance from the heart, influences negatively the amplitude of the ECG signal. According to [12], large voltages are recorded in the precordia leads in comparison with the unipolar limb leads.

Clinical interpretation of ECG is useful in many applications including diagnosis of arrhythmias, ischemia, myocardial infraction, and so on. However, proper instrumentation and technical specifications are required and have been proposed by the American Heart Association and the Association for the Advancement of Medical Instrumentation.

EEG

The Austrian psychiatrist Hans Berger was the first one to record the human EEG in 1929, and since then this bioelectric signal has been the most utilized to clinically monitor brain function [13]. An EEG is a superposition of many different bioelectric sources in the outer cortex that generate measurable oscillations of brain electric potential from the human scalp [14, 15]. These signals are generally difficult to decode since they translate the activity of billion of neurons diffused via brain tissues, fluids and scalp. However, EEG is still a useful tool to detect pathologies such as brain tumors, epilepsies, infectious diseases, head injuries and sleep and metabolic disorders [16].

The brain is a complex organ with massive bioelectrically active neurons and with three primary divisions: brainstem, cerebellum and cerebrum. The largest part of the brain is the cerebrum, and can be divided into the right and left hemispheres, each relating to the opposite side of the body. The surface layer of each hemisphere is called the cerebral cortex, containing about 10^{10} nerve cells (neurons) and believed to generate most of the electrical activity measured on the scalp. The cortex represents the processing unit for sensorial and motor signals, receiving sensory information from the skin, eyes, ears and other receptors [15, 17]. There are four functional sub-divisions or lobes of the cerebral cortex, as shown in Figure 2.4.

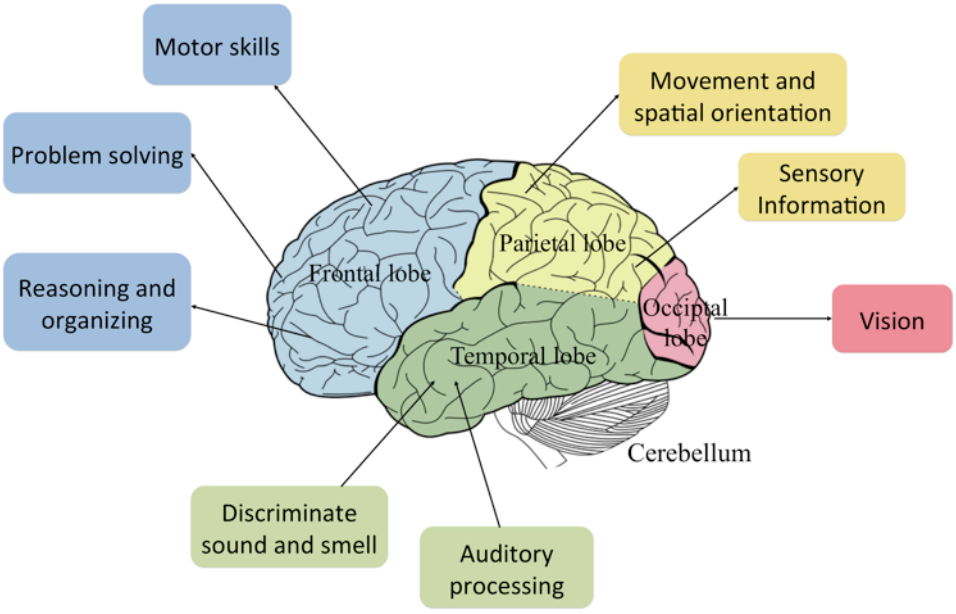

Figure 2.4 Brain main lobes and associated functions.

As shown in Figure 2.4, the fissures are the major dividing landmarks of the cerebral cortex resulting in four lobes: frontal, occipital, parietal and temporal. Each one of these lobes can be connected with a different function such as auditory, motor or visual. The front part of

the brain is called frontal lobe and is involved in reasoning, motor skills, organizing, problem solving and a variety of higher cognitive functions such as behavior and emotions. The visual system is mainly controlled by the occipital lobe and is located at the back portion of the brain. This lobe is responsible to interpret visual stimuli and information from the eyes. The parietal lobe is associated with the integration of sensory information from different parts of the body and is located in the middle section of the brain. General functions of this lobe include movement, spatial orientation, speech, pain and touch sensation. The bottom region of the cortex is called the temporal lobe, and can be divided into two parts, each located on both sides of the skull. The temporal lobe is responsible to coordinate auditory processing, interpreting sounds and language, as well as to distinguish and discriminate smell and sound [17, 18].

Electrical activity measured in the scalp can be divided into two types: spontaneous potentials (example: beta or alpha rhythms) and evoked potentials or event-related potentials [15]. The latter is the direct response to some external stimulus like an auditory tone or a visual signal, whereas event related potentials are dependent on the brain processing of the stimulus. Properties such as frequency, amplitude and recording site are often used to characterize spontaneous EEG waveforms. EEG spectral analysis allows to associate each pattern with certain mental states such as sleep or consciousness [16]. Major brain rhythms are categorized according to their predominant frequency components and can be classified as: alpha, beta, delta, gamma and theta waves. Figure 2.5 shows frequency characteristics and mental states associated with each EEG waves.

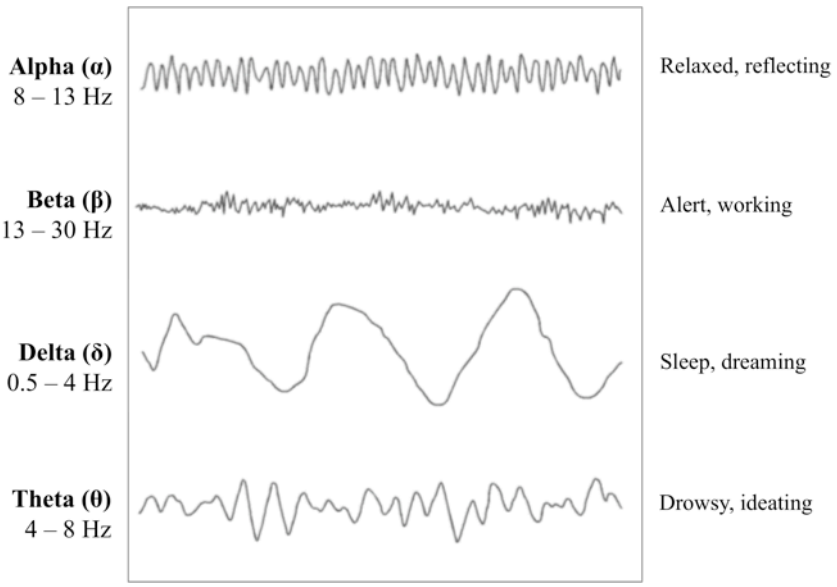

Figure 2.5 EEG brain waves according to different states of consciousness (adapted from [16]).

There is a progression of EEG activity from a state of wakefulness to deep sleep, which reflects mainly on a decrease of frequency and increase in amplitude. Alpha rhythms are characterized by frequencies of 8 to 13 Hz and typical of an awake, quiet and resting state of consciousness. These waves have higher amplitudes on occipital and frontal areas of the brain, being the typical value below 50 μV in adults. On the other hand, beta waves have smaller amplitudes (20 μV) but higher frequency components ranging from 14 to 30 Hz. These waves are more frequently recorded from the parietal and frontal regions of the brain and are particularly present during intense mental activity. There's also a higher-frequency EEG wave called gamma that is characterized by frequencies above 35 Hz and amplitudes of 3 to 5 μV. Gamma waves are usually accompanied by sudden sensory stimuli. Waves from 4 to 7 Hz are called theta waves and occur mainly in the parietal and temporal lobes. These waves have amplitudes of 20 to 100 μV and are typical of complex behaviors such as learning and memory. As for delta waves, these have standard amplitudes of 20 to 200 μV and frequencies below 3.5 Hz. Delta eaves occur in deep sleep, coma or serious organic brain diseases [15, 16, 19].

Similarly to ECG, EEGs are also recorded according to a lead system that includes several electrode's location around the subject scalp called 10-20 lead system (Figure 2.6).

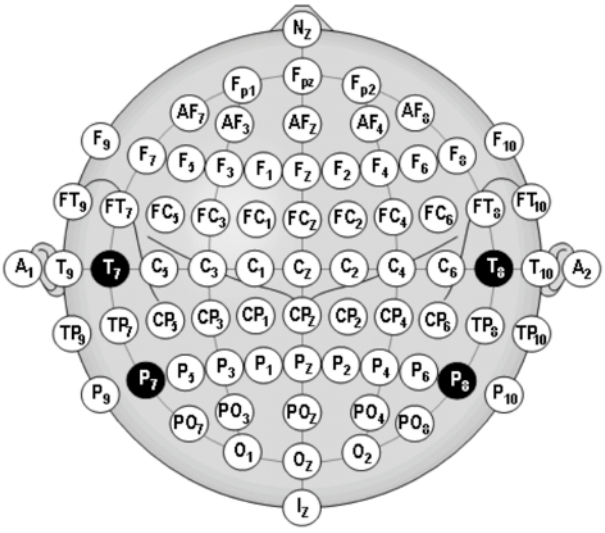

Figure 2.6 International 10-20 system of EEG electrode placement [16].

Electrodes are labeled by letters according to their positions on the scalp, i.e. depending on the monitored brain region (e.g. frontal or occipital). The 10-20 lead system consists on a diagnostic and preventing tool widely used in the study of sleep patterns, effects of various pharmaceuticals on sleep, epilepsy among others. The electrode selection influences the magnitude of the signals recorded, which ultimately influences the required sensitivity of the

sensor. In a study developed by Charles Epstein and Gail Brickley, it was found that EEG amplitude increased monotonically until a maximum inter-electrode distance of 15 cm [20].

EMG

Bioelectric activity of muscles or myoelectric activity (EMG) was first measured in 1890 by Marey [21]. EMG is generated by activation of muscles prior to contraction and is a result of the summed action potential of individual muscle motor units (MU). Since each muscle contraction involves a large number of cells, the bioelectric current flowing through the fibers gives origin to skin potentials in the range of millivolts [22].

Skeletal muscles are composed by thousands of muscle fibers that are defined as a complex multinucleated cell of variable length (from mm to cm). Muscle fibers are arranged in a parallel configuration to one another and bundle together by connective tissue, which is responsible for providing support and unity of action. MUs comprise the functional units of a muscle contraction and are composed by a group of muscle fibers innervated by one motor neuron [21]. When a neural signal is sent to a motor unit, each MU is contracted resulting in a synchronous activation of all the innervated muscle fibers. EMG signals represent the spatio-temporal summation of this electrical activation of the mechanical system of muscle fibers. These signals represent the level of activity of a specific muscle and are characterized by a stochastic noise assuming a Gaussian distribution function [1]. Figure 2.7 shows that EMG can be related with the strength of an intentional muscle contraction and respective force.

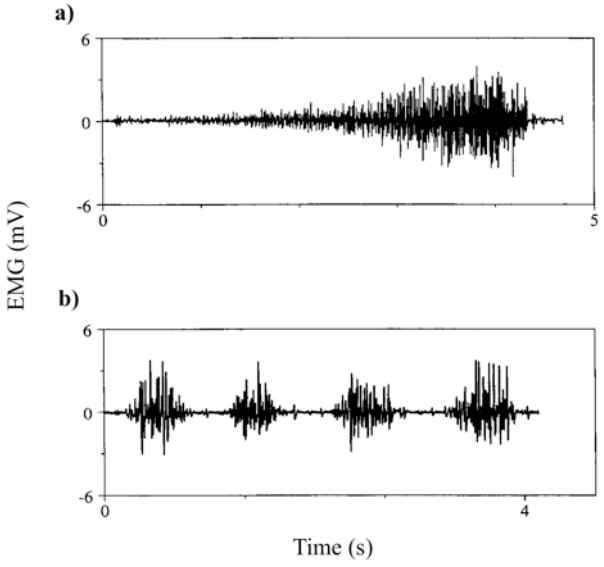

Figure 2.7 EMG signals from a) a static contraction and b) a series of contraction and relaxation [21].

EMG signals are recorded using surface electrodes placed near the muscle groups, preferably between a motor point and the tendon insertion, or between two motor points.

Electrodes should be aligned in a longitudinal midline of the muscle, being this axis parallel to the fiber length. An instrumentation or operational amplifier can be used to perform differential acquisition, similarly to ECG. EMG signals can be related with the applied muscle force. For instance, at muscle fatigues the frequency spectrum of EMG signals shifts towards lower frequencies and has smaller amplitudes. However, its frequency and amplitudes manifest minor changes over a range of low contractile force and progressive large force. According to several studies, an increase in the inter-electrode spacing produces an increase in the EMG medium magnitude [23, 24]. Although this results in difficulties in signal analysis, EMGs are still widely used as a monitoring and diagnostic tool of neuromuscular diseases (eg. Myopathy). In particular, EMG frequency-spectrum analysis finds applications in biomechanics research in order to design controlled prosthetic devices or to detect the degree of muscle fatigue and performance.

EOG

The movement of the eyeballs within the conductive environment of the skull gives origin to an electrical potential – EOG. In order to understand the generation of this bioelectric signal, the eyeballs are considered as dipoles, and electrodes are placed on each side of the eyes, above or below them. Therefore, EOG represents the dipolar current flow from the cornea to the retina, which allows to estimate the eye's angular displacement. Figure 2.8 shows an example of an EOG taken from an healthy subject [1].

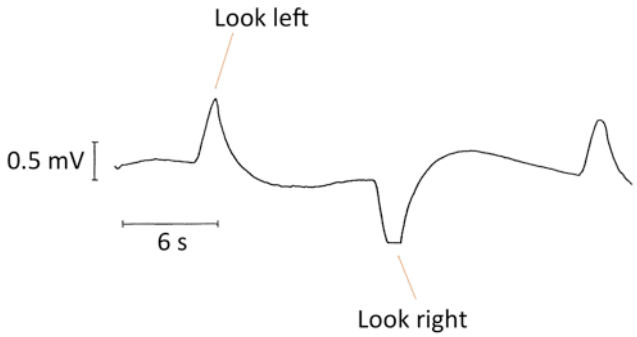

Figure 2.8 Example of an EOG signal obtained with three electrodes [1].

Figure 2.8 shows the clear positive and negative signal peaks that represent the blinking of the eyelids. Clinical applications of EOG include study of disorders of eye movement and balance, sleep and dream research, visual fatigue and evaluation of reading ability. In addition, EOG could also be used in wearable devices for instance in activity recognition and context-awareness [4].

2.2.3 Bioelectric Signals Main Properties and Challenges

Measurement of bioelectric signals involves recording very low voltage and low frequency signals, with high impedance sources, overlaid with interference and noise signals. Essentially, bioelectric signals are associated with various forms of energy and can be characterized as a function of time and space [1, 4]. Therefore, this allows for a non-invasive acquisition of such signals providing vital clues as to normal or pathological functions of organs. Table 2.1 lists the most important bioelectric signals measured from the body, as well as the significant properties.

Table 2.1 Types of bioelectric signals and main characteristics [1, 2, 7, 14, 19].

Bioelectric signal	Biological Source	Amplitude	Frequency
Electrocardiogram (ECG)	Heart	0.5 – 4 mV	0.05 – 150 Hz
Electroencephalogram (EEG)	Brain	5 – 300 μV	0.5 – 150 Hz
Electromyogram (EMG)	Muscles	1 – 10 mV	0 – 10 kHz
Electroocculogram (EOG)	Eye dipole field	10 – 100 μV	0 – 10 Hz
Electroretinogram (ERG)	Eye retina	0 – 900 μV	0 – 50 Hz
Electrocortigram (ECoG)	Exposed surface Brain	-	100 Hz – 5kHz
Electroneurogram (ENG)	Nerve blunder	5μV – 10 mV	100 Hz – 1kHz
Evoked potentials	Brain	0.1 – 20 μV	-
Action potentials	Nerves and muscles	-80 – 80 mV	10 – 10 kHz

Signal Amplitude and Power

Most demanding signals, such as ECG, EEG and EMG are within the μV range, often going from 5 μV to 10 mV. Giving such small amplitudes, it is very easy to have a few millivolts superimposed on the measured bioelectric signal, mainly due to power-lines. This is a major problem since magnitude and power of both signals is in the same order (Table 2.1). Likewise, other bioelectric signals lie in the same range of amplitude, resulting in further interference among signals. As an example, ECG or even EOG signals usually appear overlapped on EEG signals. Bioelectric signal amplitudes presented in Table 2.1 represent the values obtained for surface detection, and near the place or source that they are originated. In general, the human body may be considered as a volume conductor, which makes possible to

detect some bioelectric signals in different places in the body. For instance, an ECG can be detected by placing the sensors near the subject wrists, despite the compromise of reduced signal strength when compared with signals obtained near the heart. In addition, since bioelectric signals are measured as a difference of potential between two points, the distance between them interferes with the magnitude of signals detected. Therefore, the design of wearable bioelectric systems requires proper location selection for the measurement electrodes. For instance, the inter-electrode distance influences the bioelectric signal strength, i.e., amplitude.

The maximum power transfer occurs when the source impedance equals the input impedance of the measurement device. In this case, impedance matching occurs. For complex impedances, matching occurs when the conjugate are equal in magnitude. However, since bioelectric signals are within the μV range, it's important to maximize also the voltage produced in the high-impedance load. The main problem with bioelectric signal acquisition is their low power due to the small source currents. This is a problem mainly when implementing power line noise cancelation. The interference is canceled, but the bioelectric signals are also attenuated. This means that any small current flowing to the measurement apparatus will lead to a voltage drop on the transducers, reducing further the available output voltage.

Signal Frequency

From Table 2.1, it's perceptible that bioelectric signals are not difficult to measure regarding spectral components. In fact, maximum frequency is on the order of a few kilohertz. The main problem is related with smaller frequency components, close to DC, which is severely influenced by 1/f noise (or pink noise). This noise is inversely proportional to frequency. In addition, bioelectric signals have overlaying spectral components, specially centered in the range of 1 to 100 Hz, causing mutual interference between them. Even simple patient movement, which occurs on the order of a few Hz, interferes with signals such as ECG and EEG. Another common problem is associated with electromagnetic fields coming from power-lines (50 – 60 Hz) that are easily coupled through the power source or by the human body working as an antenna. This coupled signal usually has higher amplitude than the bioelectric signal being measured, which leads to the need to remove the effect of picked-up interference.

2.2 Standard Bioelectric Signal Acquisition System

The phenomenon of bioelectricity involves ions as charge carriers and its recording deals with the transduction of these ionic currents into electric currents. This type of interface is carried out by surface electrodes, consisting of electrical conductors in contact with the aqueous ionic solutions. Different electrodes are used for the recording of bioelectric signals, based on specific transduction schemes: wet, dry and capacitive electrodes. This section is going to focus on the principles of bioelectric transduction and electrode design.

Surface bioelectric signals are small in amplitude due to the impedance barrier created by the electrode-skin interface, leading to more susceptibility to artifacts. These artifacts are a result of the relative motion of the electrode and the skin, the activity of the nearby muscles and other instrumentation and environmental factors [2]. Proper signal amplification is crucial when acquiring bioelectric signals, as well as minimizing artifacts resultant from environmental and biological sources. Since bioelectric signals acquisition systems are usually used in critical-care environments and in high-fidelity applications, they must fulfill a set of requirements and components.

Figure 2.9 shows a standard bioelectric signal acquisition setup, which includes signal transduction, amplification, processing and conditioning.

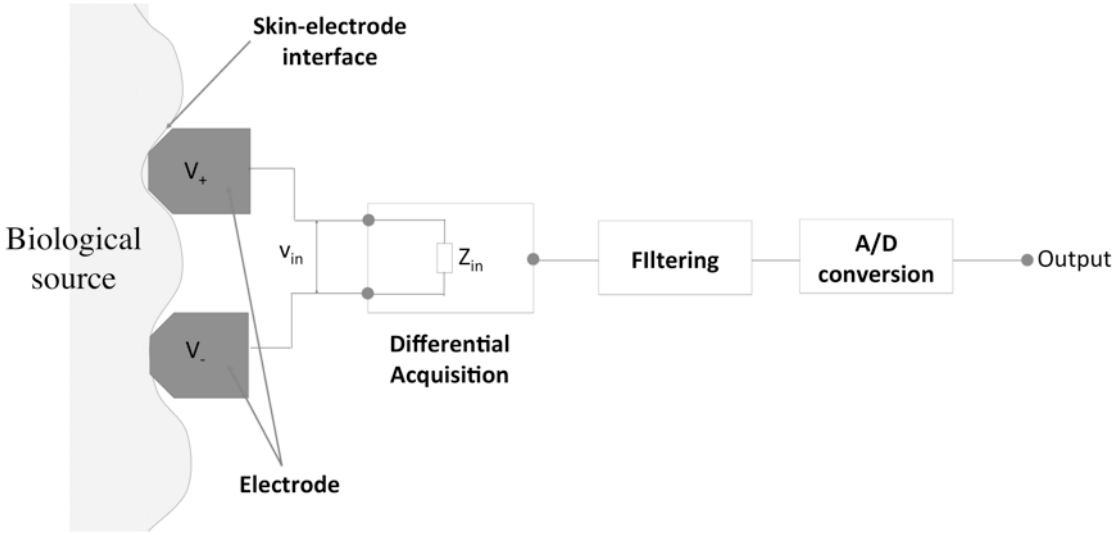

Figure 2.9 Bioelectric signal acquisition typical setup.

The differential amplifier deals with the amplification of the bioelectric signal, without compromising signal integrity. Since the input signal of the amplifier consists of the desired bioelectric signal and unwanted components (e.g. power line interference signals or other bioelectric signals), it is fundamental to include a filtering stage [25]. Generally, a notch filter

centered at 50 Hz (60 Hz in USA), and a bandpass filter are used to remove these unwanted signal components, that sometimes have higher amplitudes than the desired bioelectric signal. Finally, the setup usually includes an A/D converter to allow digital processing and communication with other units of the system and/or external devices, such as portable monitors, personal digital assistant (PDAs), among others [26].

2.2.1 Skin-electrode Interface

The charge-transfer mechanism giving origin to bioelectric acquisition takes place at the skin-electrode interface and it's of major importance in improving the design of bioelectrodes [3]. Skin-electrode interface can be modeled considering the different layers of the skin and the electrode-electrolyte interface. Generally, it is settled that the skin impedance is a combination of resistance and capacitance arranged in parallel or in series [3, 27]. This means that skin-electrode impedance is frequency dependent, and inversely related to frequency. Webster and Neuman suggested a double time constant model to describe the skin-electrode interface, as shown in Figure 2.10 [3].

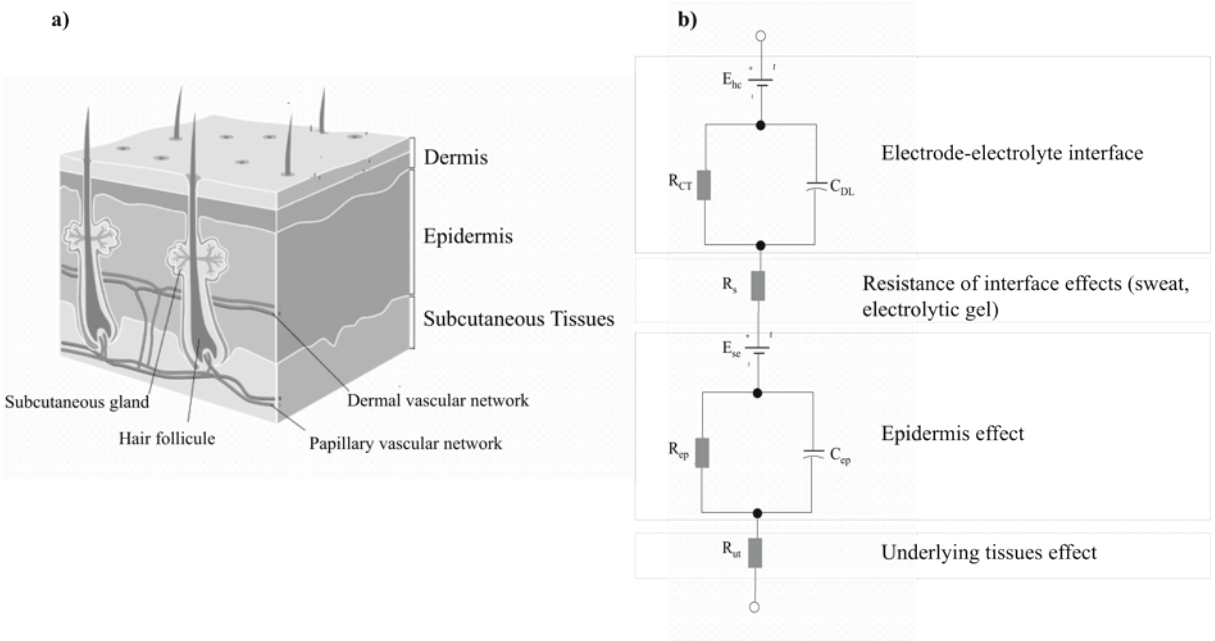

Figure 2.10 a) Human skin cross section. B) Skin-electrode interface and equivalent circuit for wet and dry electrodes**.**

As shown in Figure 2.10a, skin consists of three main layers: Epidermis, Dermis and Subcutaneous Layer [28]. The first corresponds to the outermost layer that is constantly renewing itself and whose role is crucial in the interface between the skin and the electrode. Also, epidermis provides a protective barrier against the hostile environment. The epidermis

is traversed by different skin additions (eg. hair follicles, sweat glands) and can be subdivided into the following layers: *stratum corneum, stratum granulosum and stratum germinativum.* The second layer of the skin, dermis, is well vascularized and contains a number of receptors for touch, temperature and pain. Dermis is composed by a dense network of connective tissue (collagen fibers), which results in higher elasticity and strength from behalf of the skin. The final layer, beneath the dermis, is called subcutaneous layer and acts a cushion to protect organs beneath the skin, as well as a fat storage [3, 28]. All layers, with the exception of the *stratum corneum*, have a rich composition of live tissue and ionic species that facilitate the conduction of electrical current [3, 4].

Figure 2.10b shows the impedance associated the electrode-electrolyte interface that includes the parallel between the reactive (C_{DL}) and resistive (R_{CT}) components. This impedance will be explained in detail in the next section. The series resistance R_s corresponds to the effective resistance associated with interface effects of the gel/sweat between the electrode and the skin. The flow of ionic current through the epidermal layer can be represented by a parallel RC circuit between C_{ep} and R_{ep}. The underlying tissues of the epidermis can be collectively represented by a pure resistance R_{ut} [3, 27]. The total impedance for the equivalent circuit is then defined as:

$$Z_T = R_{ut} + \frac{R_{ep}}{1+j\omega C_{ep}R_{ep}} + R_s + \frac{R_{CT}}{1+j\omega C_{DL}R_{CT}} \tag{2.5}$$

The electrode-skin interface could be approached by a capacitor with the *stratum corneum* forming the dielectric layer, since it stands between the electrode surface and the underlying tissues that from the second capacitor plate [29]. If so, the skin's capacitance will vary with *strantum corneum's* thickness, dielectric constant, and electrode area, as follows:

$$C = \varepsilon_r \varepsilon_o \frac{A}{d} \tag{2.6}$$

where ε_r is the relative static permittivity, ε_o is the medium permittivity, A is the area and d is the distance between capacitor plates. Nevertheless, throughout this thesis, skin-electrode impedance is represented in its more discretized form as shown in Figure 2.10b.

A different model can be developed for capacitive coupled electrodes, as shown in Figure 2.11.

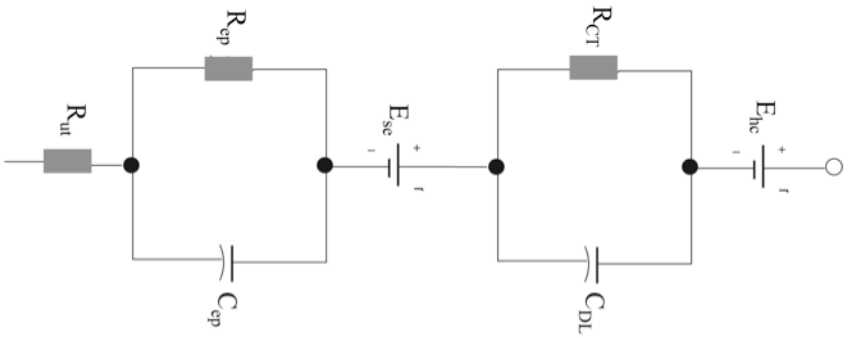

Figure 2.11 Skin-electrode interface and equivalent circuit for capacitive electrodes.

Since there isn't any electrical contact when using capacitive coupled electrodes, R_s disappears. Despite being capacitive, we consider a parallel RC circuit to electrically represent the electrodes, since we must consider always the loss component of a dielectric material. However, the frequency dependent component has the major contribution for the electrode impedance.

From the literature, we can find values for skin impedance, determined for a skin area of 1cm^2, from a frequency of 1 Hz to 1 MHz [30]. Figure 2.12 shows the frequency-dependent skin impedance that varied from 10 kΩ to 1 MΩ, at 1 Hz.

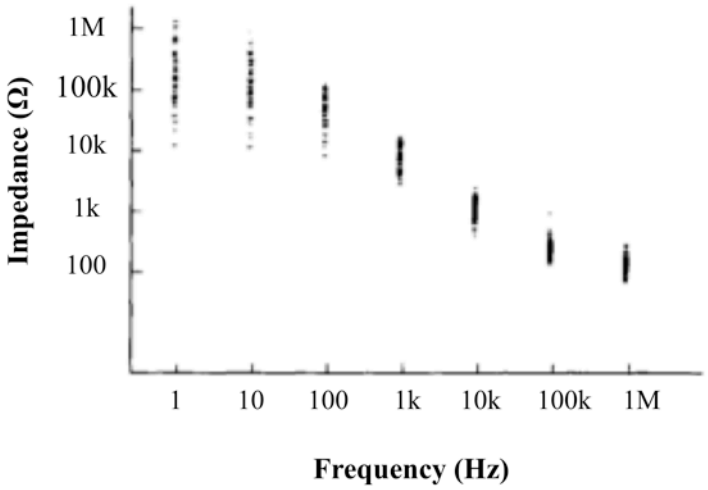

Figure 2.12 Skin-electrode impedance as a function of signal frequency [30].

Skin-electrode impedance varies with time and with recording conditions according to a set of factors, as for example: type and area of electrode, time of application, skin condition and electrolyte composition. It is recommended that skin-electrode interface for conventional wet electrodes should have an impedance below 5 kΩ, in order to maintain a reliable

contact [31]. To achieve this, skin is often cleaned and sometimes abraded in order to improve the stability of the bioelectric signal. However, this abrasion can sometimes be uncomfortable for the patient and even give rise to skin irritations. Considering an unprepared skin and the use of pre-gelled disposable electrodes, the reported values for skin-electrode impedance are in the order of 50–70 kΩ [32, 33]. As for the capacitive coupled electrodes, the skin-electrode impedance is usually in the range of hundreds of kΩ to a few MΩ [34].

2.2.2 Bioelectrodes

Transduction of bioelectric signals is performed by bioelectrodes, specially designed to obtain the signal of interest while reducing the potential to pick up artifact. The contact between an electrode and an electrolyte, such as in the saline environment of the human skin, results in electrochemical reactions. These are responsible for promoting the flow of electric current from the interface into the electrode wire; otherwise it would be impossible to measure a bioelectric signal with a recording apparatus [3].

The design of bioelectrodes must focus on reducing the contact impedance, improving signal acquisition while reducing the likelihood to pick up artifacts. In the past few decades, different bioelectrodes have been developed and can be classified according to material conductivity or functionality. If an electrode material is conductive, bioelectrode is classified as resistive since it establishes an electrical contact with the skin. On the other hand, capacitive electrodes are made of insulated materials that form a capacitive coupling with the skin [3, 27, 34]. Bioelectrodes can also be classified according to the type of transduction mechanism: passive (with no signal conditioning) or active (local signal processing).

Ohmic Contact Electrodes

Resistive electrodes can be subdivided into two main categories, depending on the type of interface between the electrode and the skin: wet and dry electrodes. The first type refers to electrodes that use an electrolytic gel solution to form a conductive path between the electrode and the skin. The electrolytic gel main function is to reduce skin-electrode impedance. The problem with electrodes made from electrically conductive metals as silver, copper or aluminum, resides in the fact that these are electrochemically reactive in electrolytes, and therefore, fail to provide a good pathway to electrolytic solutions or tissue. The best electrode materials are a combination of metals and their metallic salts, such as silver (Ag) in combination with a chloride coating (Cl). The result is the common and widely used Ag/AgCl bioelectric signal electrodes [3, 27].

Metal plate electrode, in its simplest form, consists on a metallic conductor in contact with the skin and an electrolyte solution. An example of this type of electrodes consists in adhesive disposable wet electrodes widely used in majority of clinical settings. Most recent metal plate electrodes are composed of a disk of plastic foam material with a silver-plated disk on the bottom surface, and a conductive lead attached to the electrodes. This attachement is made by a snap in the top surface of the plate. The electrolyte solution may be applied during the attachment procedure, or it can be already incorporated in the electrode – pre-gelled electrodes. Floating electrodes, on the other hand, have an electrolyte-insulated cavity that surrounds the metal disk, preventing interfacial instabilities due to motion artifacts [3, 4, 27].

Long-term usage of wet electrodes leads to a series of disadvantages, mainly originated from the electrolyte solution. In fact, although electrolytic solutions are effective in promoting a good skin contact, they also originate a source of noise in form of an electrical potential called skin diffusion potential [27, 29]. In addition, the reliance of an electrolyte leads to reduced signal quality due to gel dehydration, requiring reapplication of gel. Most importantly and considering a continuous monitoring for wearable applications, the application and removal of electrolytic solutions is an unpleasant and time-consuming procedure for the user and for the clinician. The use of pre-gelled electrodes can be an alternative in order to save time, but the patient would still be in contact with electrode gel that ultimately can lead to skin irritation [3, 4, 27].

Dry electrodes seek to overcome the limitations of wet electrodes, and often consist on a noncorroding metal such as stainless steel, as well as of conductive rubbers that can be repeatedly washed and reused. This metal is in direct contact with the skin and use the subject's own sweat to replace the artificial electrolyte [4, 27]. For this reason, dry electrodes tend to have better performances as perspiration accumulates in its surface, which results in a decrease in interface impedance with time [34]. Such an electrode has advantages when used in a wearable context, where patients may forget to apply electrolytic solution to the gels prior its use.

Capacitive Electrodes

Another category of bioelectrodes consists in capacitive electrodes that are characterized by the absence of electrical contact with the skin. These electrodes consist of a metal or semiconductor with a thin dielectric layer between it and the skin, which results in a capacitive coupling mechanism. When using capacitive electrodes, its surface is defined as one plate of a capacitor, and the skin is considered as the second plate [27, 34]. In addition,

there is no contact between the metal and the electrolyte, which means that in principle no half-cell potential is developed. Therefore, one source of noise during bioelectric signal acquisition is eliminated. Nevertheless, capacitive electrodes are still restricted by its intrinsic noise originated by charge accumulation and by the need for extremely high impedance readout circuits. In addition, any displacement of the electrode towards the body originates an artifact due to change of capacitance.

Usually, dry and capacitive electrodes are considered as active electrodes, whereas wet conventional transducers are called passive electrodes. In fact, the absence of electrolytic gel often implies to use active electrodes in order to transform high source impedance (skin) to a low source impedance (active electrode output). This results in the minimization of power-line hum. Other types of electrodes can be categorized, such as flexible or rigid electrodes. Flexible electrodes are the ones with adaptation ability to the inhomogeneous structure of the human skin. Examples of such electrodes are textile electrodes or other polymeric material that serves as an electrode. Novel dry and textile-based wearable electrodes have been recently proposed. These include for example conductive rubber electrodes [35], Cu sputtered textile electrode [36], conductive fabric sheets and Polyvinylidene Fluoride (PVDF) film electrodes [37], polymeric dry electrode [38].

Electrical Equivalent Model

Electrochemical reactions resultant from electrode-electrolyte interface consists in ionic solution redox, i.e. oxidation-reduction. Basically, when current flows from the electrode towards the electrolyte, oxidation occurs, being the opposite called reduction. Under equilibrium, rates of both reactions are balanced, and therefore, the current flowing in one direction is equal and cancels the current flowing in the opposite direction. Although this net current flowing is zero, due to the ion concentration fluctuations on the vicinity of the interface, a potential difference occurs known by half-cell or reversible potential [3, 27]. This potential depends on a set of parameters such as temperature, ions concentration and electrode material. The half-cell potential (E_{hc}) is particularly important in measurements involving low frequency or DC signals. Ideally, differential electrodes should have a cell potential difference of zero, i.e. their individual E_{hc} should be the same [3, 27]. However, wearable bioelectric signal electrodes are subjected to oxidation due to air exposure, staining or previous electrolyte exposure, which results in unbalanced E_{hc}. In consequence, an offset potential is added to the bioelectric signals being measured, which amplitude can reach several tens or

hundreds of millivolts. Electrode offset potentials causes current through the electrodes and through the signal conditioning circuit, being often mistaken with bioelectric potential [4, 29].

Electrical characteristics of bioelectric signal electrodes are generally nonlinear and sensitive to current density at their surface. In fact, during charge transition between the electrode and electrolyte, many must first diffuse to the interface, leading to a double layer of charge. Therefore, an interface capacitance (C_{DL}) is often included in the equivalent circuit model that characterizes the electric characteristics of the electrode-electrolyte interface (Figure 2.13a) [3, 27].

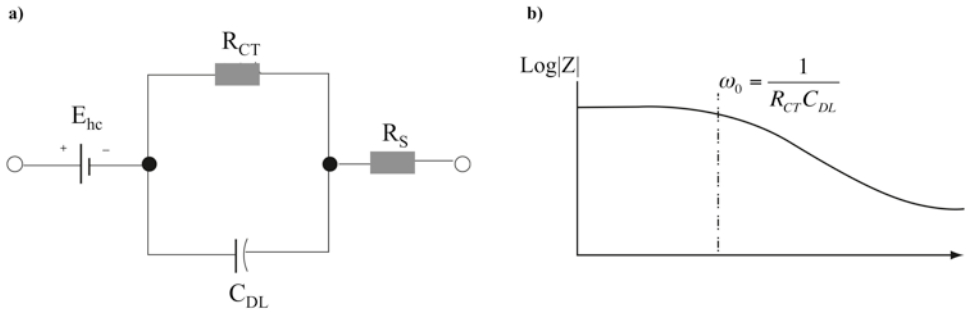

Figure 2.13 a) Equivalent circuit of bioelectric signal electrode–electrolyte interface; b) Impedance plot for equivalent circuit.

The equivalent circuit in Figure 2.13a comprises a RC parallel that represent the resistive (R_{CT}) and reactive components (C_{DL}) of the impedance associated with the electrode-electrolyte interface. The resistive component can be considered as a charge transfer resistance that shunts the nonfaradaic C_{DL}. The remaining elements correspond to the E_{hc} and a series resistance (R_s), which is essentially related with the electrolyte resistances. The electrode-electrolyte equivalent circuit demonstrates a frequency –dependent behavior, as shown in Figure 2.13b. At lower frequencies, the magnitude of the interface impedance is merely resistive since it consists on a sum of the contributions of R_s and R_{CT}. On the other hand, as frequency increases the capacitive impedance decreases whereas C_{DL} bypasses R_{CT}. Therefore, R_s dominates and equals the magnitude of the electrode-electrolyte impedance. At frequencies between these two limits, the electrode impedance is frequency dependent and thereby influenced by C_{DL}. This frequency dependency has little impact on bioelectric signal acquisition since bioelectric signals such as ECG, EEG or EMG have lower frequency components.

From an electrical outlook, a good bioelectrode should have a very low value for the resistive component, since it implies free charge transfer as well as a slight voltage drops across the interface. However, electrode-electrolyte resistance depends on several physical

properties as electrode composition, surface area and polarization. Typical skin electrodes have electrode-electrolyte resistance on the order of hundred ohms [3].

2.2.3 Bioelectric Signal Amplification

Bioelectric signal amplification is required to make it compatible with a variety of devices such as A/D converters or display equipment. These signals are recorded using a differential recording device that can be generally described as:

$$v_{BIO} = A_{diff}(v_+ - v_-), \tag{2.7}$$

where A_{diff} is the differential gain and where v_+ and v_- are the electrical potential on each of the noninverting and inverting inputs of a bioelectric signal amplifier, respectively.

A typical configuration for a bioelectric signal amplifier is called instrumentation amplifier that combines the main desirable features for this type of measurements. Instrumentation amplifiers are designed to have extremely large input impedances, high differential gain and ability to reject common signals at the differential inputs, such as power lines interference [4, 25]. This signal is often called common-mode voltage, and good instrumentation amplifier for bioelectric signal recordings requires the strong rejection of this signal. Nowadays, complete instrumentation amplifier integrated circuits (IC) are commercially available. Different considerations can be assumed depending on the type of bioelectric signal to measured. In fact, each one has a particular characteristic that makes the amplifier more prone to amplify or to remove common interference [2, 25]. Table 2.2 shows some of the special design considerations and features to take into account, during amplification stage design.

Table 2.2 Bioelectric signal-specific features and design considerations (adapted from [2]).

	Specific Features	**Design considerations**
ECG	mV level signal, Bandwidth (BW) of 0.05 – 150Hz.	Moderate gain, noise, CMRR, input impedance
EEG	Lower amplitude signals (microvolts)	Higher gain (>10000), low noise, higher input impedance and CMRR
EMG	Higher BW, higher amplitudes	Smaller gain, post-acquisition data processing

2.2.4 Bioelectric Signal Sensor Transfer Function

The relationship between each input of the recording device, considering the total impedance (Z_T) and the amplification stage input impedance (Z_{in}), can be described as:

$$v_{+or-} = v_{BIO+or-} \frac{Z_{in}}{Z_{in}+Z_T} \tag{2.8}$$

According to (2.8), Z_{in} of a bioelectric signal amplifier must be sufficiently high in order to avoid the attenuation of the bioelectric signal under measurement. The complete models can now be described for each approach and for the different recording situations, having in mind that the difference between them is the total impedance Z_T, which changes according to each type of electrode.

Considering the use of wet electrodes, Z_T is given by (2.5) and v_- and v are easily find. For instance, for v_-:

$$v_- = v_{BIO-} \frac{Z_{in}}{Z_{in}+\left[R_{ut}+\frac{R_{ep}}{1+j\omega C_{ep}R_{ep}}+R_s+\frac{R_{CT}}{1+j\omega C_{DL}R_{CT}}\right]}. \tag{2.9}$$

The same can be done for v_+, since a balance between the electrodes is assumed. Wet and dry electrodes are expected to have the same electrical model although the impedances values will be significantly different. In this case, R_s is related with the interface with electrode and sweat produced by the epidermal layer.

The overall bioelectric signal sensor transfer function is obtained substituting (2.9) in (2.7). As a result, for wet and dry electrodes:

$$v_{BIO} = A_{diff}(v_{BIO+} - v_{BIO-}) \frac{Z_{in}}{Z_{in}+\left[R_{ut}+\frac{R_{ep}}{1+j\omega C_{ep}R_{ep}}+R_s+\frac{R_{CT}}{1+j\omega C_{DL}R_{CT}}\right]}. \tag{2.10}$$

2.3 Wearable Bioelectric Acquisition Systems

At this point, bioelectric signals were described as well as the requirements for the acquisition of each signal. Although the essential acquisition components are similar for stationary or ambulatory monitoring, several requirements and characteristics need to be

defined for wearable applications.

2.3.1 System Components

The design of a wearable system implies three areas of work that need to be properly covered. First, it's important to develop unobtrusive wearable sensors to reliably record bioelectric data. Second, these sensors need to be implemented into a substrate material that allows for multi-sensor integration. And finally, it's important to provide infrastructures to extract and transmit data, in order to improve system performance at a clinical level and enhance mobility in individuals [39, 40].

Figure 2.14 depicts an architectural layer for an ideal wearable bioelectric system, which is composed of a functional/smart substrate, embedded electronics and attachable peripherals/appliances.

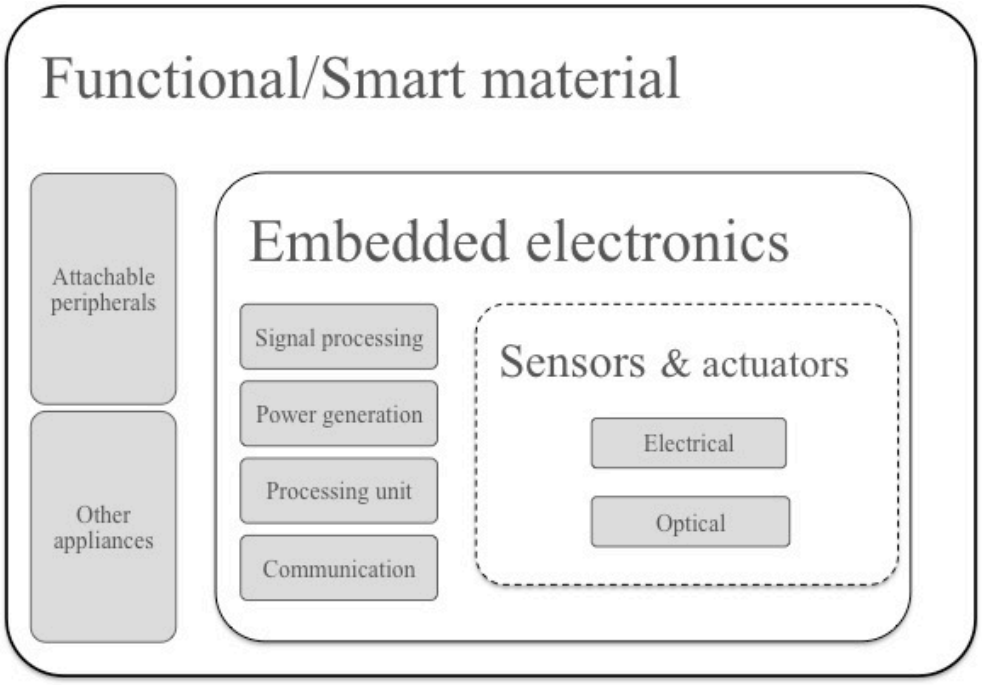

Figure 2.14 Architectural layer of an ideal wearable bioelectric system

Wearable system components may be divided into three main categories: clothing in form of a smart or functional material, embedded components, and attachable peripherals [40, 41]. The first includes all the substrate materials that act as a functional or smart structure by providing necessary supporting elements for devices that are not directly attached to the human body. Substrate materials allow the embedment of sensors, signal processing units and communication infrastructures, among others. In addition, they are responsible to provide protection from environmental conditions such as temperature changes

and humidity. The most common substrate materials used in wearable systems are textiles or flexible polymeric materials that will enable the design of normal garments with multifunctional nature [42-44]. Two approaches can be followed: one where electronic and optical components are attached into conventional clothing and accessories; or by integrating them during the manufacturing process. The latter allows creating truly functional fabrics that can be crushed and washed, whereas their properties are unaffected [40].

The embedded components include all the necessary electronics, optics, or other, that will provide sensing, actuating, signal processing, communication infrastructures, power generation, and other desired functions [40, 41]. Focusing on the sensing technologies, new approaches are required specially in providing non-contact methodologies that will improve the embedment of these components. In addition, this would contribute to the design of totally wearable and highly comfortable functional garments. Sensors are used to monitor all the necessary physiological parameters and physical environment surrounding the user, allowing to maintain the user's health condition. They can be either embedded or the material itself works as a sensing element [40, 45].

If necessary and desirable, attachable peripherals and other appliances can be included into the wearable system. Examples of these types of components are: PDAs, displays, keyboard and control knobs. Since most of peripherals are not robust enough to resist clothing-typical handling like washing and drying, they are usually associated with a particular piece of clothing or an accessory.

2.3.2 Wearability Requirements

The design of bioelectric signal acquisition for wearable devices isn't very different from regular instrumentation, despite the fact that it must fulfill the set of requirements stated in Chapter 1. Here, the main characteristics in terms of wearable systems concept and design towards maximizing the wearability will be discussed.

Wearability is classified according to a set of requirements such as low weight, small size and comfort. The main goal is to provide a device that can be carried and/or worn. The selection of the wearable material that will serve as a substrate is of extreme importance, since it determines the wearability depth, as well as the aesthetics and comfort of the device. Ideally, the substrate material used should be flexible and based on textile materials since it's possible to design systems with higher similarities to common garments. Elastic textiles or knits are the eligible materials due to their skin fitting capabilities that eventually leads to a minimization of motion artifacts and electrode displacement [46].

Location of sensors is also a major influence towards wearability, since user movements can affect the performance of the overall system. For instance, if placing the electrodes near main muscles, the muscle and movement artifact are prone to be a negative influence in the final output. In addition, the wearable system should be noninvasive, comfortable and unobtrusive, which limits the positioning of the different bioelectric sensors. The criteria selected for sensor placement depends on the functionality and accessibility needed. Nevertheless, recommended areas are those subjected to low movement and with large surface area. For instance, a sleeveless garment can be adopted for cardiac monitoring since it avoids the problems associated with limb's movements. Flexibility and applicability of the wearable system are improved if having the ability of scalability, i.e. add or remove components from the garment [46, 47].

The device should be able to interact with the environment through a network of sensors placed in different parts of the clothing or accessories. This allows to create a certain alertness of the physiological and emotional state of the user, as well as the surrounding environment. Data handling, decision support and feedback are also crucial to establish a good interaction between the device, the components and the user itself. In order to properly interact with the user, the interface should meet the principles of simplicity and friendliness, whereas minimizing the user's cognitive effort and its intervention during the process [39].

Reliability plays an important role for medical devices, especially those designed for dealing with life-threatening situations or long-term monitoring without clinical intervention. Continuous breakdowns reduce functionality of wearable devices and often lead to frustration and reduce usage on behalf of the patients.

2.3.3 Performance Requirements

Wearable system performance is driven by a set of factors related mainly with the bioelectric signal sensors used. The more general requirements are related with communication and interconnection, power supply and on-board processing. These factors are inter-dependent since the use of communication and on-board processing will increase the complexity of the system. In consequence, the power consumption will increase, affecting the autonomy of the device. Therefore, a trade-off must be established between these factors, envisioning sensor performance maximization, in terms of power autonomy.

One of the most common problems in measuring bioelectric signals is the noise and interference usually superimposed in the signal of interest. In fact, since used in a variety of situations and environments, wearable bioelectric devices are subjected to different

interference sources. Table 2.3 gives an overview of the main artifacts involved in wearable bioelectric signal acquisition systems, with indications of the peak-to-peak voltages that can be induced. It's important to determine the maximum peak-to-peak noise level acceptable mainly for ECG and EEG, since they are the most demanding signals in terms of sensitivity. Criteria selection for this threshold can be for instance considering 1% of the typical amplitudes recorded for each signal. Therefore, the acceptable noise level for ECG and EEG can be considered as 10 μV and 1 μV, respectively [29].

Table 2.3 Sources of Interference in wearable bioelectric signal recording.

Source	Magnitude fields	Frequency components
Home appliances	220 V	50 – 60 Hz
Lighting	10 kV/m	1 Hz – 1 kHz
Portable phones	1 W/m^2	>500 MHz
Microwave ovens	50 W/m^2	2.45 GHz
Skin motion artifact (stretching of the skin)	5 – 15 mV	DC
Thermal noise	0.5-10 μV	Equivalent bandwidth of the measurement device
Electrode movement	0.1 – 1000 μV	<1 Hz
Electrode-electrolyte (typical)	0.2 – 10 μV	
Skin-electrolyte interface	10 – 80 μV	

The above table shows that the most noteworthy artifacts affecting bioelectric signal acquisition is the interference from environmental sources unavoidably present in clinical or daily routine situations. In fact, since the human body is a good conductor, it acts as an antenna, coupling the electromagnetic radiation resultant from: 50/60 Hz power lines, fluorescent lighting and other equipment. The power lines interference causes intolerable noise levels in most bioelectric signals since they have components in the 50 – 60 Hz spectral band. It is very easy to have a few millivolts superimposed on the measured signal due to the power lines, which is of the same order of magnitude as the bioelectric signal itself. This interference represents a problem mainly regarding the power supply of the electronic

components used. To avoid this, batteries can be used as power supply, which eliminates the AC and DC fluctuations caused by common power line supply. However, 50/60 Hz interference may also be electromagnetically coupled to the body through electrical cables and interconnections [2, 29].

Another problem during signal acquisition is associated with subject activity, which has frequency components inside the frequency band of interest, introducing the so-called movement artifacts. These artifacts can be manifested in several forms such as skin motion artifact or electrode displacement (electrode movement, electrode-electrolyte) [27, 29]. Unbalanced effects on each electrode, also causes severe interference in bioelectric signal recordings. To eliminate this, it's important to use high input impedance measurement devices, as described in (2.10).

The overall induced body potential due to these noise and interference sources, are present at both inputs of the differential amplification stage, which can be called as common-mode potential (V_{cm}). Therefore, it is valuable to eliminate this voltage in order to prevent saturation or over-contamination of the signal of interest. In order to successfully eliminate interference or common-mode potential, it's important to design amplification systems with a high common-mode rejection ratio (CMMR) [25] . This characteristic measures the capability of the amplification system to reject interference that is equally presented at both inputs.

The overall considerations for bioelectric signal acquisition systems for wearable systems are [2, 25]:

- Supply enough gain within its bandwidth in order to reach an output level compatible with the remaining system;
- High input impedance to prevent the attenuation of the bioelectric signal, and to prevent them to be altered by other impedances variations, such as electrode impedance;
- High CMRR (> 80 dB) in order to separate as much as possible the relevant signal from noise and interferences;
- Have low output impedance and supply the amount of current necessary to the load.

Although existent technologies fulfill most of these requirements, problems associated with integration, flexibility and immunity to some interferences, such as Magnetic Resonance Imaging (MRI) rooms or others, are still a challenge.

2.4 Wearable Photonic Systems

A way to overcome the limitations imposed by electronic wearable systems mainly regarding with system integration and functionality, is the use of optical fiber–based sensors. Nowadays, optical fiber–based sensors offer the possibility of measuring other physiological signals, such as temperature, activity and blood pressure [48, 49]. In addition, optical components are already integrated in several materials and using different techniques, compatible with current textile technology [50].

2.4.1 Main Properties

Photonic technologies are based on light modulation and use optical fibers to transport it. As stated in Chapter 1, optical-based sensors have advantages when compared with electrical counterparts. An important requirement to be eligible to bioelectric signal monitoring is the ability to detect electric fields or voltages. Optical–based sensors are able to do this and to function correctly in environments where electrical interconnections fail to succeed, such as MRI rooms. Optical–based sensors are immune to electromagnetic interference, which opens the landscape of possible applications of these sensors [48, 49, 51]. In fact, it's possible to design all-optic suits with attachable power supply units in plug-in modules that can be taken off when entering in such electromagnetic interference susceptible environments.

Optical-based sensors offer the possibility of performing contactless measurements of electrical signals. This can be achieved using transducer effects by which a material exhibits an electro–optic (EO) response in the presence of a stimulus such as an external electric field (Table 1.1). By avoiding the existence of contact between the sensor and the skin, more practical and dynamic wearable solutions are available. In fact, the ideal solution is to provide the maximum comfort and flexibility to the user.

2.4.2 Main Applications

Photonic sensors are used in a variety of applications since they are able to measure different parameters such as mechanical (force, pressure, temperature), electrical and magnetic, or chemical and biological. In this thesis, the focus is towards electrical measurements. Photonic technologies are widely available for high-speed communication systems, which main areas of applications are in the military, aerospace and

telecommunication networks. All these technologies are applied to sense electric fields or to use a specific voltage signal to modulate light in order to produce EO switches.

Although photonic systems allow to eliminate the majority of electrical components and interconnections used, other optical components have to be considered. A set of requirements must be taken into account when selecting the appropriate photonic technology to use in the wearable bioelectric acquisition device. Some of these properties are shown in Table 2.4, for each type of EO modulating devices based on optical fiber [48].

Table 2.4 Photonic sensors comparison considering wearability (adapted from [48]).

	Microbending	**Macrobending**	**Michelson Interferometer**	**Mach-Zehnder Interferometer**	**Pockels/Kerr effect**
Shape	Simple	Flexible			Simple
Placement	Dependent on the final application				
Size/Weight	Small / light		Small to medium/Light to medium		-
Electronics / other optics	Simple / none		Moderately complicated / Beam Splitter, coupler	Moderately complicated / Beam Splitter, coupler, mirrors	Depends on the optical components / Polarizer
Advantages	Simple, multi-sensing	Simple, versatile	Versatile geometry, multi-sensing		-
Drawbacks	Mechanical damage of the fiber, (force) Cross-sensitivity	Mechanical damage of the fiber (bend) Cross-sensitivity	Laser needed, unknown application for low frequency signals		Unknown structure

2.4.3 Photonic Bioelectric Systems Principle

At this point, wearable bioelectric signal systems requirements were exposed, as well as the advantages of using optical–based sensors for electric field measurements. Therefore, combining the possibility of measuring electrical signals, with the wearability provided by optical-based sensors, it's possible to design systems with higher performances in a wearable bioelectric detection context.

Photonic sensors for electric field measurement operate by modulating light passing through the optical fibers, according to the effect of an external electric field [52]. This modulation can be classified according to external or intrinsic modulation, being the main different related with their names: the use of an external device to modulate light [49].

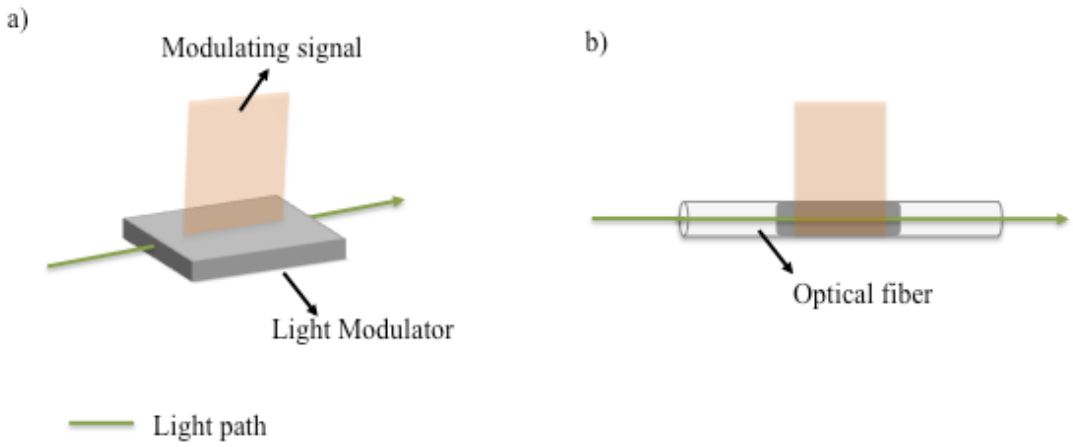

Figure 2.15 a) Extrinsic and b) Intrinsic light modulation schemes.

A modulation is called intrinsic when the optical signal source and the modulator are in the same device, i.e. optical fiber (Figure 2.15a). In this case, devices are called all-fiber sensors, and the entire fiber length is used as the sensitive area. Extrinsic or hybrid modulation consists on using the optical fiber only as a light carrier. Light is further modulated by an external optical device, as shown in Figure 2.15b. Modulated light is then carried to an optical detector. In opposition to direct modulation, extrinsic sensors performance is driven by the nature of the sensing device, instead of the optical fiber material. The main drawbacks over intrinsic modulation are the increase in production costs and complexity, as well as an increase in the overall device size. Nevertheless, extrinsic modulation is the preferred technique in this work, since it offers a higher control over the modulation [49, 53].

Depending on which property of light is modulated, modulation can be classified as intensity, phase, frequency or polarization modulation. As the name indicates, the modulation category corresponds to the light property modified by the environmental change or signal, i.e. bioelectric signal. Intensity modulation is one of the most used techniques in EO modulators, since intensity variations are more easily detected and converted to an electrical value [52, 53].

References

[1] J. W. Clark Jr, "The origin of biopotentials," in *Medical instrumentation: application and design*, 2nd ed., J. G. Webster and J. W. Clark, Eds. John Wiley & Sons, 1995, pp. 126-188.

[2] N. Thakor, "Biopotentials and electrophysiology measurement," in *The Measurement, Instrumentation, and Sensors Handbook*, vol. 74, John G. Webster, Ed. Springer, 1999.

[3] M. Neuman, "Biopotential electrodes," in *Medical Instrumentation: application and design*, 2nd ed., J. G. Webster and J. W. Clark, Eds. John Wiley & Sons, 1995, pp. 183-232.

[4] B. C. Towe, "Bioelectricity and its measurements," in *Standard Handbook of Biomedical Engineering and Design*, M. Kutz, Ed. McGraw-Hill, 2004, pp. 17.3 - 17.50.

[5] J. Malmivuo and R. Plonsey, *Bioelectromagnetism: Principles and Applications of Bioelectric and Biomagnetic Fields*, vol. 20, no. 6. Oxford University Press, 1995.

[6] C. Zywietz, "A Brief History of Electrocardiography - Progress through Technology," *Distribution*, 1888.

[7] E. J. Berbar, "Principles of Electrocardiography," in *The Biomedical Engineering Handbook*, 2nd ed., vol. 15, J. D. Bronzino, Ed. CRC Press LLC, 2000, p. 236.

[8] K. A. Mackenzie, "Clinical Electrocardiography," *British medical journal*, vol. 2, no. 11, p. 145, 1953.

[9] M. A. S. Ali, X. P. Zeng, and G. J. Li, "Electrophysiology and Biopotential Issues on Human Electrocardiogram-A Review," *American J. of Engineering and Applied Sciences*, vol. 4, no. 3, pp. 313-319, 2011.

[10] W. Einthoven, "Galvanometrische registratie van het menschilijk electrocardiogram," *Herinneringsbundel Professor SS Rosenstein*, pp. 101-107, 1902.

[11] M. Puurtinen, J. Viik, and J. Hyttinen, "Best electrode locations for a small bipolar ECG device: signal strength analysis of clinical data.," *Annals of biomedical engineering*, vol. 37, no. 2, pp. 331-6, Feb. 2009.

[12] P. W. Macfarlane, *Comprehensive Electrocardiology*, vol. 33, no. 2. Pergamon Press, 2011, p. 1792.

[13] H. Berger, "Das Elektrenkephalogramm des Menschen," *Naturwissenschaften*, vol. 23, no. 8, pp. 121-124, 1935.

[14] J. A. V. Bates, "Fundamentals of Electroencephalography," *Journal of Neurology, Neurosurgery & Psychiatry*, vol. 42, no. 1, p. 146, 1972.

[15] P. L. Nunez and R. Srinivasan, *Electric fields of the brain*. Oxford University Press US, 2006, p. 484.

[16] E. Niedermeyer and F. H. L. D. Silva, *Electroencephalography: Basic Principles, Clinical Applications, and Related Fields*, vol. 1. Lippincott Williams & Wilkins, 2004, p. 1309.

[17] S. Boniface, "Atlas of Electroencephalography," *Journal of Neurology, Neurosurgery & Psychiatry*, vol. 59, no. 3, p. 452, 1995.

[18] W. J. Hendelman, *Atlas of functional neuroanatomy*, vol. 1, no. 1. CRC Taylor & Francis, 2006, p. xxi, 270.

[19] J. D. Bronzino, "Principles of Electroencephalography," in *The Biomedical Engineering Handbook*, 2nd ed., J. D. Bronzino, Ed. CRC Press LLC, 2000.

[20] C. M. Epstein and G. P. Brickley, "Interelectrode distance and amplitude of the scalp EEG.," *Electroencephalography and Clinical Neurophysiology*, vol. 60, no. 4, pp. 287-292, 1985.

[21] K. Heinrichs, "Introduction to Surface Electromyography," *Journal of Athletic Training*, vol. 10, no. 1, p. 69, 1999.

[22] G. S. Rash, "Electromyography Fundamentals," *http://myweb.wwu.edu/~chalmers/EMGfundamentals.pdf*, 2008. [Online]. Available: http://myweb.wwu.edu/~chalmers/EMGfundamentals.pdf.

[23] A. Melaku, D. K. Kumar, and A. Bradley, "The influence of Inter-Electrode Distance on EMG," *Electromyography and clinical neurophysiology*, vol. 41, no. 7, pp. 437-42, 2001.

[24] T. W. Beck et al., "The effects of interelectrode distance on electromyographic amplitude and mean power frequency during isokinetic and isometric muscle actions of the biceps brachii," *Journal of Electromyography and Kinesiology*, vol. 15, pp. 482-495, 2005.

[25] J. H. Nagel, "Biopotential amplifiers," in *The Biomedical Engineering Handbook*, 2nd ed., J. D. Bronzino, Ed. CRC Press LLC, 2000.

[26] D. Prutchi and M. Norris, *Design and development of medical electronic instrumentation: a practical perspective of the design, construction, and test of medical devices*. John Wiley & Sons, 2005.

[27] E. McAdams, "Bioelectrodes," *Encyclopedia of Medical Devices and Instrumentation*, vol. 148, no. 1. John Wiley & Sons, pp. 120-165, 2006.

[28] E. N. Marieb and K. Hoehn, *Human Anatomy & Physiology*, vol. 70, no. 4. Pearson Benjamin Cummings, 2007, p. 1159.

[29] E. Huigen, "Noise in biopotential recording using surface electrodes," no. November, 2000.

[30] J. Rosell, J. Colominas, P. Riu, R. Pallas-Areny, and J. G. Webster, "Skin impedance from 1 Hz to 1 MHz," *IEEE Transactions on Biomedical Engineering*, vol. 35, no. 8, pp. 649–651, 1988.

[31] D. K. Swanson and J. G. Webster, "A model for skin-electrode impedance," in *Biomedical Electrode Technology*, H. A. Miller and D. C. Harrison, Eds. New York: Academic, 1974, pp. 117-128.

[32] M. M. Puurtinen, S. M. Komulainen, P. K. Kauppinen, J. a V. Malmivuo, and J. a K. Hyttinen, "Measurement of noise and impedance of dry and wet textile electrodes, and textile electrodes with hydrogel.," *Conference proceedings : ... Annual International Conference of the IEEE Engineering in Medicine and Biology Society. IEEE Engineering in Medicine and Biology Society. Conference*, vol. 1, pp. 6012-5, Jan. 2006.

[33] R. S. Khandpur, *Handbook of Biomedical Instrumentation*. Tata McGraw-Hill Education, 2003, p. 944.

[34] A. Searle and L. Kirkup, "A direct comparison of wet, dry and insulating bioelectric recording electrodes.," *Physiological measurement*, vol. 21, no. 2, pp. 271-83, May 2000.

[35] C. Yong Ryu, S. Hoon Nam, and S. Kim, "Conductive rubber electrode for wearable health monitoring.," *Conference proceedings : ... Annual International Conference of the IEEE Engineering in Medicine and Biology Society. IEEE Engineering in Medicine and Biology Society. Conference*, vol. 4, pp. 3479-81, Jan. 2005.

[36] S. Jang, J. Cho, K. Jeong, and G. Cho, "Exploring possibilities of ECG electrodes for bio-monitoring smartwear with Cu sputtered fabrics," *HumanComputer Interaction Interaction Platforms and Techniques*, vol. 4551, pp. 1130-1137, 2007.

[37] S. Choi and Z. Jiang, "A novel wearable sensor device with conductive fabric and PVDF film for monitoring cardiorespiratory signals," *Sensors and Actuators A: Physical*, vol. 128, no. 2, pp. 317-326, Apr. 2006.

[38] J. Baek, J. An, J. Choi, K. Park, and S. Lee, "Flexible polymeric dry electrodes for the long-term monitoring of ECG," *Sensors and Actuators A: Physical*, vol. 143, pp. 423-429, Nov. 2007.

[39] X.-F. Teng, Y.-T. Zhang, C. C. Y. Poon, and P. Bonato, "Wearable Medical Systems for p-Health," *IEEE Reviews in Biomedical Engineering*, vol. 1, pp. 62-74, 2008.

[40] D. I. Fotiadis, C. Glaros, and A. Likas, "Wearable Medical Devices," in *Wiley Encyclopedia of Biomedical Engineering*, John Wiley & Sons, Inc., 2006.

[41] P. Lukowicz, T. Kirstein, and G. Tröster, "Wearable systems for health care applications.," *Methods of information in medicine*, vol. 43, no. 3, pp. 232-8, Jan. 2004.

[42] A. Lymberis, "Intelligent biomedical clothing for personal health and disease management: state of the art and future vision," *Telemedicine Journal and e-health*, vol. 9, no. 4, 2003.

[43] F. Carpi and D. De Rossi, "Electroactive polymer-based devices for e-textiles in biomedicine," *Information Technology in Biomedicine, IEEE Transactions on*, vol. 9, no. 3, pp. 295–318, 2005.

[44] S. Park and S. Jayaraman, "Smart textiles: Wearable electronic systems," *MRS bulletin*, vol. 28, no. 8, pp. 585–591, 2003.

[45] A. Bonfiglio, *Wearable Monitoring Systems*. Springer Verlag, 2010.

[46] F. Gemperle, C. Kasabach, J. Stivoric, M. Bauer, and R. Martin, "Design for wearability," *Digest of Papers. Second International Symposium on Wearable Computers (Cat. No.98EX215)*, pp. 116-122.

[47] a Pantelopoulos and N. G. Bourbakis, "A Survey on Wearable Sensor-Based Systems for Health Monitoring and Prognosis," *IEEE Transactions on Systems, Man, and Cybernetics, Part C (Applications and Reviews)*, vol. 40, no. 1, pp. 1-12, Jan. 2010.

[48] J. Rantala, J. Hännikäinen, and J. Vanhala, "Fiber optic sensors for wearable applications," *Personal and Ubiquitous Computing*, vol. 15, no. 1, pp. 85-96, Jun. 2010.

[49] K. Address, "Fiber optic sensors and their applications," *Symposium A Quarterly Journal In Modern Foreign Literatures*, pp. 1-6, 2009.

[50] E. Bosman et al., "Fully Flexible Optoelectronic Foil," *IEEE Journal of Selected Topics in Quantum Electronics*, vol. 16, no. 5, pp. 1355-1362, Sep. 2010.

[51] A. Grillet et al., "Optical Fiber Sensors Embedded Into Medical Textiles for Healthcare Monitoring," *IEEE Sensors Journal*, vol. 8, no. 7, pp. 1215-1222, Jul. 2008.

[52] B. E. A. Saleh and M. C. Teich, *Fundamentals of photonics*, vol. 45, no. 11. Wiley-Interscience, 2007, p. 1177.

[53] A. Seeds and K. Williams, "Microwave photonics," *Journal of Lightwave Technology*, vol. 27, no. 3, pp. 314-335, 2006.

Chapter 3

Photonic Bioelectric Signal Sensor

This chapter addresses the whole photonic bioelectric signal sensor modeling and design, including optical and electrical component selection. The ultimate goal is to design a photonic platform that will perform electro-optic (EO) conversion of the bioelectric signal into an optical modulated signal. The EO stage herein described comprises the optical signal generation, EO modulation and photodetection.

3.1 Photonic Sensor Theory

In this section, the theory behind the EO effect will be described as well as the type of devices that exhibit this phenomena. The bioelectric signal is responsible to perform light modulation. Different devices can be use to perform EO sensing from which the most relevant

in this thesis is the Mach-Zehnder Interferometer (MZI) modulator. This device allows to perform differential measurements.

3.1.1 Linear Electro-Optic Effect

Certain materials exhibit a phenomenon called birefringence, where the orthogonal components of light polarization travel at different velocities. Therefore, for each of the two different perpendicular states of polarization, the light will travel in a different direction. This birefringence can be induced by an external electric field, giving origin to the EO effect [1], [2]. Through this effect, a time-varying applied electric field, i.e. the bioelectric signal, causes the time-dependency of refractive index of an EO substrate, by which light passes. The proportionality between the amount of change in refractive index (n) and the electric field strength (E) is described by [2], [3]:

$$n(E) = n_0 - \frac{1}{2} r_p n E - \frac{1}{2} r_k n E^2 \tag{3.1}$$

where the coefficients r_p and r_k are called the linear (Pockels) EO and second order (Kerr) EO coefficients, which values depend on the direction of the applied electric field and the polarization of the light [1]. Equation 3.1 can be simplified considering only the linear EO effect, by eliminating the quadratic component.

Only noncentrosymetric crystals exhibit the Pockels effect since the difference between applying an electric field in reverse signal should not produce the same effect on the new n. All materials display the Kerr effect, with varying magnitudes, but it is generally much weaker than the Pockels effect. These effects do not appear simultaneously, instead one of them becomes dominant [3].

3.1.2 Light Modulation Principle

The induced phase variation ($\Delta\phi$) of input light due to an external electric field can be expressed as [3, 4]:

$$\Delta\phi(t) = \frac{\pi}{\lambda} n^3 r_p v_{in}(t) \tag{3.2}$$

where λ is the wavelength of the input polarized light. The voltage needed to produce a phase shift of π is called half-wave voltage (v_π) and it influences the modulation depth. In fact, as

lower this parameter is, less voltage is required to produce a detectable change in light intensity. The v_π is defined as:

$$v_\pi = \frac{\lambda d}{n^3 r_p L} \tag{3.3}$$

where d is the electrode spacing and L the electrode length. Therefore, v_π is the standard measure of sensitivity of an EO modulator. Substituting equation (3.3) into (3.2) results in a simplification of $\Delta\phi$ produced by the modulation:

$$\Delta\phi(t) = \frac{\pi}{2v_\pi} v_{in}(t) \tag{3.4}$$

Phase variations can be manifested as intensity modulation if incorporating an interferometry design, which facilitates the conversion of the modulated optical signal into an electrical signal [3, 4]. The modulated power of the detected beam is described as:

$$P_{out} = \frac{P_{in}IL}{2}\left(1 - cos(\frac{\pi}{2v_\pi} v_{in}(t))\right) \tag{3.5}$$

where P_{in} is the input power of light and IL is the insertion loss of the EO modulator. The latter property is the result of the light loss within the modulator. The main contributors for IL are the fiber-crystal interface and propagation loss throughout the waveguides [4, 5].

3.1.3 EO Materials and Modulators

Materials that respond to an external electric field, with a change of the inherent n are called EO materials. These include glasses, crystals, semiconductor and polymers. Most used materials for photonic devices are shown in Table 3.1 [3, 5–7].

The choice of the EO material depends on the final application and the required characteristics, since each one has advantages and disadvantages. Nevertheless, the most used material for photonic applications is the ferroelectric crystal Lithium Niobate ($LiNbO_3$) [4, 8]. These crystals have high EO coefficient and low optical loss as well as thermal, chemical and mechanical stability. In addition, waveguide fabrication and miniaturization techniques of EO modulators using this material have been widely explored [5, 8]. Although semiconductor EO materials are more compact and compatible with the majority of integrated devices, the linear EO effect shows weaker values when compared with $LiNbO_3$ [4].

Table 3.1 EO materials and main properties [3, 5–7].

Material	Type of Material	Refractive index	EO coefficient (Pockels) ($x10^{-12}$ m/V)
Quartz	Glass	$n_o = 1.544$ $n_e = 1.553$	$r_{41} = 0.2$
$LiNbO_3$	Crystal/Ferroelectric	$n_o = 2.297$ $n_e = 2.208$	$r_{33} = 30.8$
Potassium Dideuterium Phosphate (KD*P)	Crystal/ Ferroelectric	$n_o = 1.5079$ $n_e = 1.4683$	$r_{63} = 26.8$
Zinc Telluride (ZnTe)	Semiconductor	$n_o = 2.99$	$r_{41} = 4.04$
Cadmium Telluride (CdTe)	Semiconductor	$n_o = 2.84$	$r_{41} = 6.8$
Polycarbonate with CDL-1 chromophore (PC-CLD-1)	Polymer	$n_o = 1.8$	$r_{33} = 70$
Poly(methylmethacrylate) with CDL-1 chromophore (PMMA-CDL1)	Polymer	$n_o = 5$	$r_{33} = 60$

Regardless of the type of material/component used, as long as they modulate light, any of them can be considered an EO modulator. Nevertheless, the most common EO modulators nowadays are based on waveguide technologies (eg. MZI Modulator) [5, 8]. In fact, using waveguide modulators allows to achieve lower v_π, which results in higher modulation efficiencies, when compared with bulk crystals.

In general, EO modulators can be divided into two categories according to the relation between light path and the measured field direction (Figure 3.1). Longitudinal modulators are those that apply the electric field along the propagation direction of light (Figure 3.1a). In this case, (3.3) can be re-written into [2, 3]:

$$v_\pi = \frac{\lambda}{2n^3 r_p} \tag{3.6}$$

On the other hand, when the signal is applied in the perpendicular direction to the light propagation, the EO modulator is called transversal (Figure 3.1b). The v_π of this type of modulators is defined as in (3.3). In $LiNbO_3$ crystals, the strongest interaction occurs between the electric field applied in the z-direction and z-polarized light, i.e., with the electric field applied transversely to the z-cut surface of the crystal [3, 5].

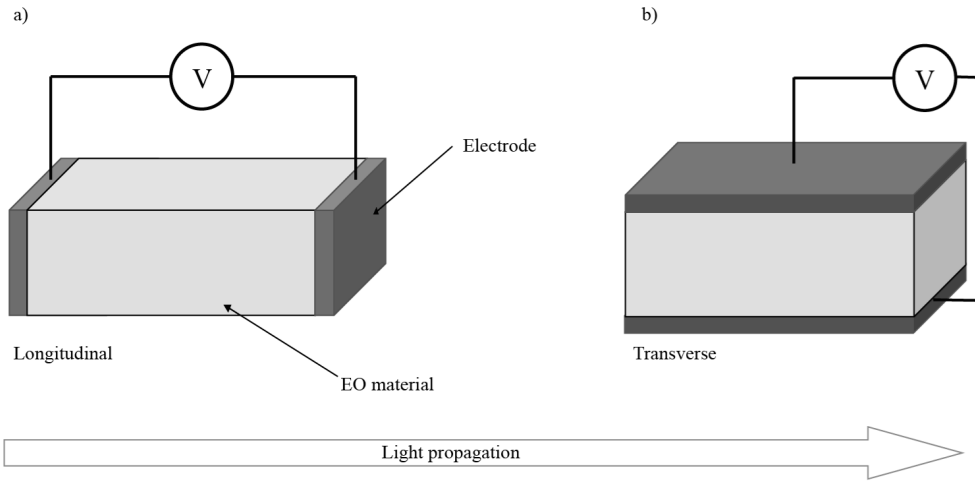

Figure 3.1 a) Longitudinal and b) Transverse EO modulation.

Although EO conversion can be performed in free-space, considering a wearable application, the modulation geometry or scheme applied should be based on waveguide technologies and optical fiber connections.

3.1.5 Mach-Zehnder Interferometer

A MZI operates first by equally splitting an optical wave into two waveguide branches that will interact with a z-polarized electric field, inducing changes in the n of the substrate material ($LiNbO_3$). When combining both waveguide legs of the interferometer, which in this case is made by a Y-branch, an interference pattern is created resulting in intensity modulation [3, 4]. Figure 3.2a) depicts this phenomenon by which the MZI modulates light intensity through the influence of an electric field.

The intensity modulation has a linear relationship with the electric field applied, if setting the modulator operation point at the linear region, i.e. quadrature point. A bias voltage (v_{bias}) is usually applied to set the MZI modulator at this point, which is the steepest part of the response curve. This means that a small change in voltage produces the maximum variation in output signal [2, 9]. The modulating signal can be applied in two ways as shown in Figure 3.2b): single drive, where only one arm of the MZI modulator is driven by the signal; or dual drive, where both paths are phase modulated.

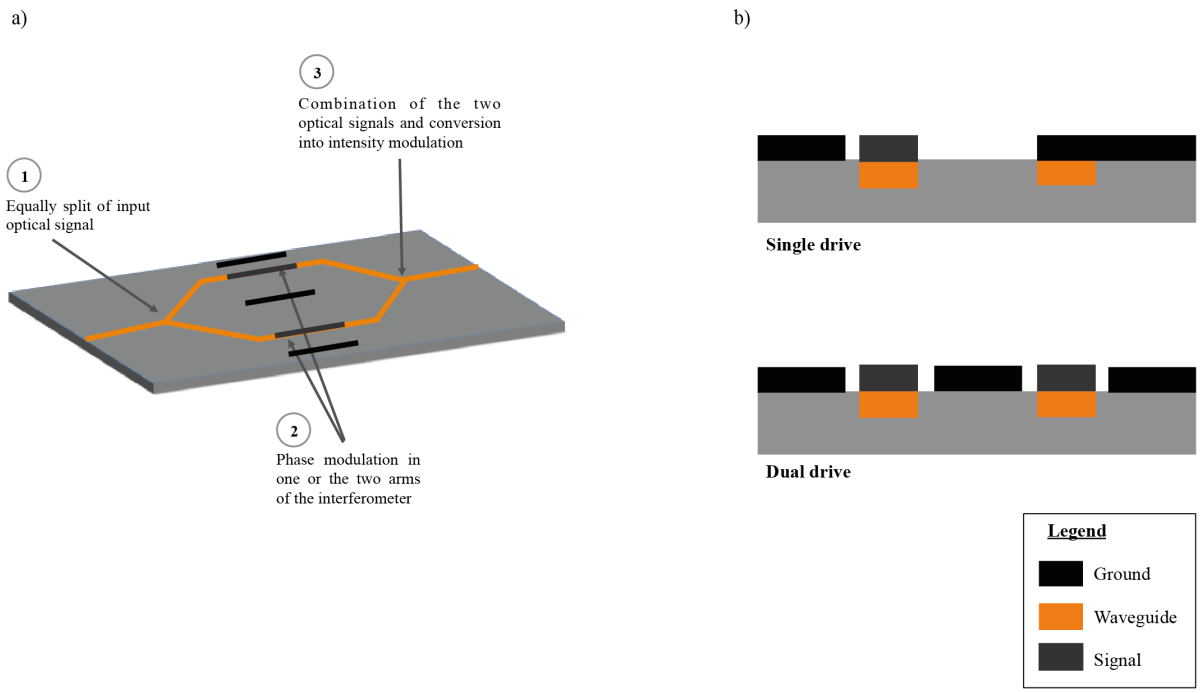

Figure 3.2 MZI a) geometry and functioning, and b) cross-section view of single and dual drive configuration.

The mechanism behind step 3 in Figure 3.2b), relies on the recombination of both phase differences that are described by equation (3.5). The net phase difference is calculated, and transformed into intensity modulation. The mechanism and figures of merit of the MZI modulator will be further discussed in the design section.

3.2 Photonic Acquisition System Architecture

The configuration of the EO sensor includes three main functional stages: optical signal generation; EO modulation and optical detection. Light is carried using optical fibers that are responsible to maintain and preserve the lightwave properties, such as polarization. Figure 3.3 depicts the configuration of the EO sensor proposed.

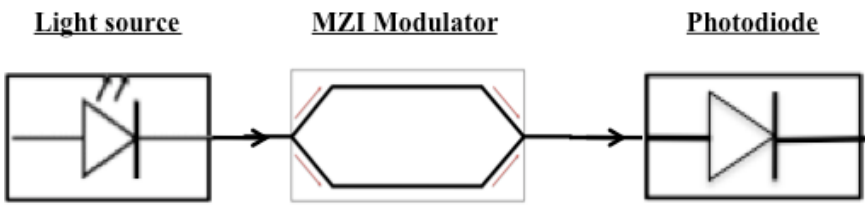

Figure 3.3 Photonic sensor design for bioelectric signal acquisition.

The proposed bioelectric signal monitoring device is based on EO acquisition technology by which an electric field is used to intensity modulate the optical signal. The photonic acquisition system includes:

- An optical signal source;
- An optical transducer to modulate the optical signal in response to a bioelectric signal;
- A detection module comprising a photodiode or an optical spectrum analyzer (OSA)

The present system has several advantages facing the conventional systems already mentioned in Chapter 2, such as: require no electronic components on the wearable garment, reducing integration complexity and allowing the use of such wearable device on specific environments like Magnetic Resonance Imaging (MRI) rooms. Also, wearable requirements such as producing an electrical output for further processing, customization and resistance to adverse conditions (e.g. regular cleaning processes), are assured.

3.3 Photonic Acquisition Stage

The design of the photonic acquisition stage involves a series of performance issues that are dependent on the components used. The performance factors consist in high modulation efficiency, adequate bandwidth, good linearity and sensitivity. The following sub-sections will discuss the design of each photonic acquisition stage component.

3.3.1 Optical signal source

The first component of the photonic system is an optical signal generator, or a light source, responsible to provide with a signal to modulate. The development of semiconductor optical devices is valuable in this field, since it allows to design more efficient and compact light sources [4, 10].

An optical signal source is characterized by several properties, being the most relevant ones the wavelength, intensity (optical power) and stability. In order to ensure the absence of optical damage on EO crystals (e.g. $LiNbO_3$), the light wavelength used should be above 800 nm, at which the photorefractive effect is generally negligible (@optical powers <100 mW) [5, 11]. The typical wavelength range used in photonic systems is around 1300 to 1550 nm (C-band), which is in the limits that prevent damage. The total power

spectrum (P_{in}) should be maximized in order to increase modulation efficiency (s_{MZI}) and in consequence sensor sensitivity. However, the upper limit of 100 mW should be taken into account. Ideally, the light source should produce a continuous wave (CW) light beam, i.e. with a stable light intensity, since it allows for a more stable operation. This is due to the influence of wavelength in the v_π of the EO modulator as translated in (3.6).

3.3.2 MZI Modulator

In this work, EO modulators perform intensity modulation since it's easier to process the resultant data and to convert it to an electrical value. In addition, following this approach, differential measurements are easily achieved through the use of interferometry mechanism, such as MZI modulators. Waveguide technology should be applied since it facilitates integration and allows to produce MZI modulators with lengths reaching the range of μm [8, 9, 11]. An example of such small MZI modulator can be found in the work developed by developed by Xueying Wang et al. (2010), where a modulator with a length of 42.6 μm and and v_π of 1.25 V was presented [12]. The main MZI figures of merit driving its performance in bioelectric signal acquisition are: electrode configuration, EO material, EO crystal orientation, v_π, s_{MZI} and linearity.

Since bioelectric signals have magnitudes from 5 μV to 10 mV and are usually recorded using a differential setup, the dual-drive configuration is recommended. By doing this, the bioelectric signal can be applied to both waveguide legs producing a push-pull effect on the light. The electric fields are opposite in effect in each path, i.e. the light traveling in one of the path is retarded, undergoing a negative phase change. On the other waveguide leg, light is advanced i.e. undergoes a positive phase change. As a result, the s_{MZI} is multiplied by a factor of two. In addition, pus-pull configuration contributes to cancel the laser-intensity noise common to both beams, improving the signal-to-noise ratio (SNR).

From the different EO materials, the material of choice is the $LiNbO_3$ due to its combination of high EO coefficient, low optical loss and compatibility with common integrated-circuit (IC) processing technology. The appropriate orientation is a z-cut crystal, i.e. transversal mode that involves placing the electrodes such that the waveguides are below them and the electric field applied is perpendicular to the z-cut surface (Figure 3.4). The design of these devices is simplified and a good thermal stability is ensured. MZI modulators that use this type of electrode configuration are called travelling-wave modulators.

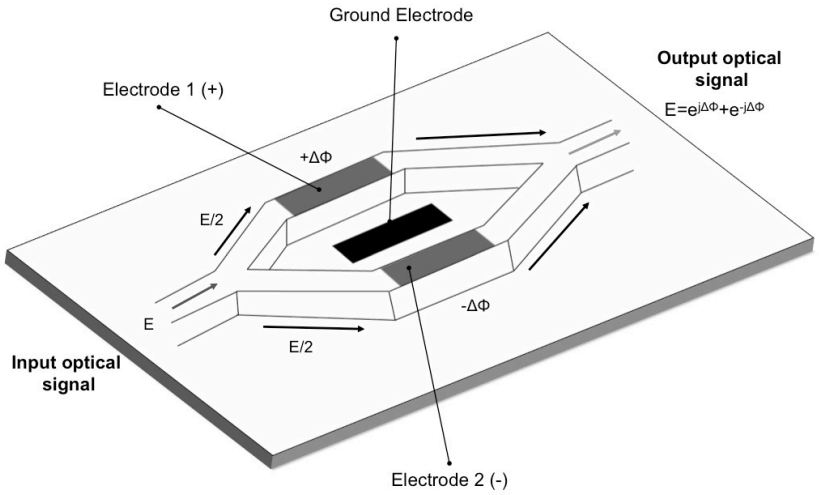

Figure 3.4 $LiNbO_3$ MZI modulator geometry**.**

Linear relationship between the intensity modulation and the bioelectric signal is obtained when the v_{bias} is set in the linear operating region, i.e. quadrature region. In order to determine the linear region, the transfer function needs to be represented in a plot (Figure 3.5) as a function of total input voltage (V_{it}). The transfer function of the dual-drive MZI modulator takes into account the overall phase change produced in each waveguide leg, and can be defined as:

$$P_{out} = \frac{ILP_i}{2}\left[1 + cos\left(\frac{\pi V_{it}}{V_\pi}\right)\right] \tag{3.7}$$

where V_{it} is the sum of v_{bias} with the bioelectric signal v_{BIO}. The modulation or slope efficiency (W/V) of the MZI corresponds to the change in the optical output power for a given change in input current, and is defined as [4]:

$$s_{MZI} = \left|\frac{dP_{out}}{dv_i}\right|_{v_{it}=0} = \frac{\pi ILP_i}{2V_\pi}\sin\left(\frac{\pi v_{bias}}{V_\pi}\right) \tag{3.8}$$

The MZI s_{MZI} depends on the v_{bias}, and can be increased by using stronger optical light sources, as shown in (3.8). However, P_{in} is limited by size and cost of power light sources, and the threshold damage of the MZI modulator. Equation (3.8) also indicates the need to reduce v_π, in order to increase s_{MZI} and in turn the gain of the photonic stage. Ideally, no external v_{bias} should be required, since it contributes to the simplicity of the photonic setup, eliminating the need for an extra DC power source or bias-specific circuit.

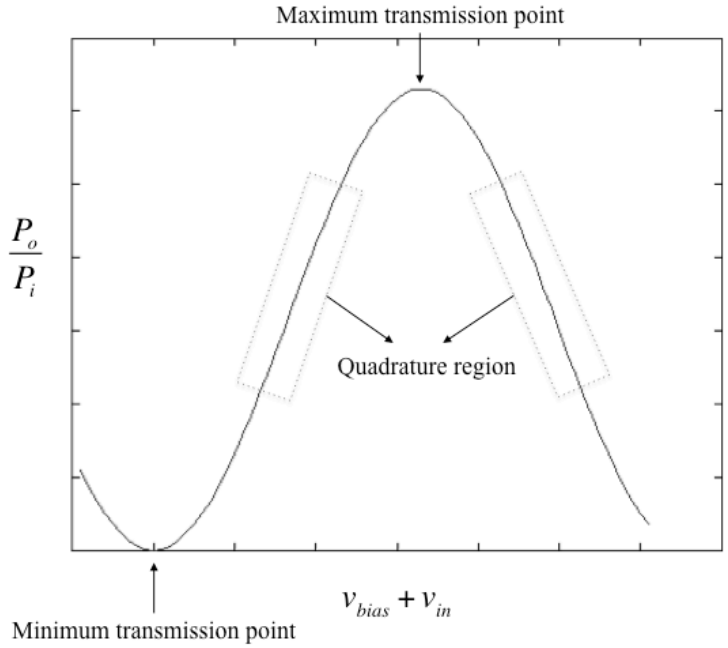

Figure 3.5 MZI transfer function obtained through (3.7), and considering an IL of 6dB and a v_{bias} from -0,2 to 6V.

As shown in Figure 3.5, the transfer function is characterized by periodic behaviour, showing that it's possible to extend the regions of linear operation to more than one option. The optimum v_{bias} should be set to half the difference between the maximum and minimum transmission point in order to maximize s_{MZI}. Also, v_{bias} can be located at any odd multiple (N) of the difference between transmission points, as in:

$$v_{bias} = N\frac{v_{maxtrans} - v_{mintrans}}{2} = N\frac{v_\pi}{2} \tag{3.9}$$

Therefore, in order to properly bias the MZI modulator, a valid v_{bias} can be selected from (3.9), and equation (3.7) and (3.8) can be linearized, yielding:

$$P_{out} = \frac{ILP_i}{2}\left[1 \pm \frac{\pi V_{BIO}}{V_\pi}\right] \tag{3. 10}$$

$$s_{MZI} = \frac{\pi ILP_i}{2V_\pi} \tag{3.11}$$

These equations allow to translate the bioelectric signal into an optical modulated signal, at the output of the MZI. Estimations and calculations for adequate and threshold values will be further detailed in section 3.5.

3.3.3 Photoreceiver

The fiber optic receiver used in the photonic sensor should be based on optoelectronic (OE) components in order to perform the reverse of EO conversion. The most common OE receiver used in photonics is the photodiode that produces an electrical current (i_{ph}) in response to the incident modulated light (P_{out}). This current signal can be further converted into a voltage signal that represents the bioelectric signal detected at the surface of the body.

Photodiodes, devices that perform photodetection, are characterized by a factor called responsivity (R), which corresponds to conversion efficiency (A/W). DC responsivity represents the slope of the characteristic transfer function of the OE conversion and in this case can be defined as [2, 10, 13]:

$$R = \frac{i_{ph}}{P_{out}} = \eta \frac{q}{h f_c} \tag{3.12}$$

where η is the quantum efficiency, q is the electron charge, h is Planck's constant and f_c is the frequency of light ($f_c = {}^{c}/_{\lambda}$). This factor is dependent on the wavelength of the light source. With the increase of wavelength, the optical power is carried by more photons resulting in higher number of electrons. Since photoelectric detectors are responsive to the photon flux rather than to the incident optical power, R increases with wavelength. The R should then be as high as possible. The best strategy to raise this value is to choose a light source with the highest wavelength as possible, and at the same time inside the allowable range of the MZI modulator. Likewise, the damage threshold of the photodiode should be taken into account.

Fiber optic technology includes two types of photodetectors: PIN diode and avalanche photodiode (APD). The most used photodetectors in photonics and for the wavelengths of interest are PIN-based detectors, due to is simple fabrication and reduced costs. PIN photodiodes can be fabricated with several substrate materials, being the most common ones based in silicium (Si) and indium gallium arsenide (InGaAs) [1, 2, 10]. The photodiode may be used in the photoconductive or in photovoltaic mode. The latter works without biasing the photodiode, becoming the most appropriate for the photonic stage herein described since it allows to design low-power consumption systems. In fact, in the photovoltaic mode there's no biasing, which means that no power is consumed for the photodetection of the intensity modulated light.

3.3.4 Other Optical Components

Since the EO effect is polarization dependent, the polarization state of the input light supplied to the modulator, must be controlled and maintained through using polarization maintaining (PM) optical fibers. In addition, single mode (SM) fibers are preferred over multimode (MM), since they provide better transmission with less distortion and cross-talk between fibers [14]. To minimize back-reflections from the fiber to the $LiNbO_3$ interface and ensure long-term stability and reliability, an angle cut and polished tube must be used to connect the input and output fibers to the modulator.

The connection between optical fibers is made through optical couplers, which operate by dividing light into two or more fibers, with possibility of selecting different coupling ratios. Nevertheless, power losses occur during each coupling mechanism, since it's difficult to ensure proper matching and alignment between each fiber core [5, 14].

3.4 Photonic System Modeling and Performance Analysis

3.4.1 Electrical Equivalent Circuit

The photonic system can be represented by an electrical equivalent circuit in order to establish a full model of the photonic platform herein presented. The equivalent circuit is depicted in Figure 3.6.

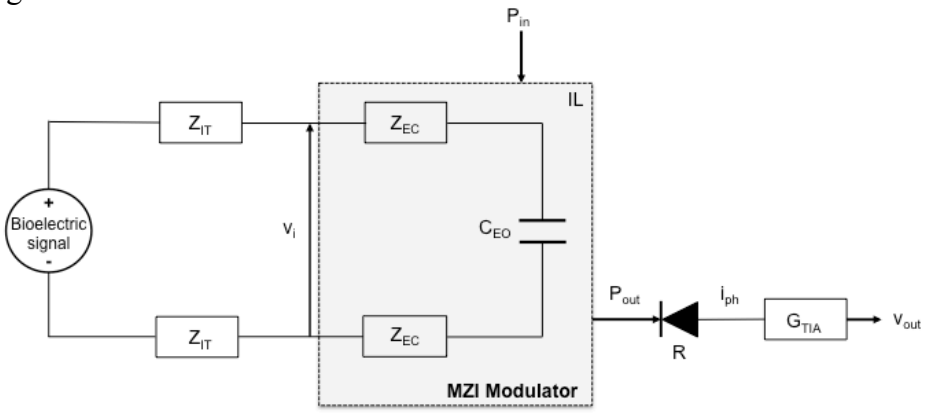

Figure 3.6 Equivalent electrical circuit of the LiNbO3 MZI modulator.

Here, the electrical model of the MZI modulator is similar to a common instrumentation amplifier, where the input impedance is represented by a capacitance (C_{eo}). The main contributors for the capacitive nature of the MZI are the insulation of the MZI terminals and

the ferroelectric nature of the $LiNbO_3$. This capacitance is dependent on the dimensional characteristics of the $LiNbO_3$ crystal and is expressed by:

$$C_{eo} = \varepsilon_0 \varepsilon_r \frac{2wl}{d_{eo}} \tag{3.13}$$

where ε_0 is the permittivity of the a vacuum, ε_r is the relative dielectric constant of the $LiNbO_3$, and w, l and d_{eo} are the width, length and distance of the crystal, respectively. Considering our application, the capacitance should be as small as possible. In this way, the input impedance of the MZI modulator will be higher, and high quality differential measurements are more likely to be performed. To minimize C_{eo}, as for any other application, the d_{eo} can be increased and w and the l decreased. This is actually a benefit for the present application, since it's desired to minimize the size of the sensor for further use in wearable applications.

The conversion efficiency of the optical detector, which includes the transimpedance gain (G_{TIA}) and the R of the photodiode, as well as the coefficient for the IL.

3.4.2 Photonic System Model

The electrical output value can be determined by a proportionality factor G_{TIA}, regarding the output current of the photodiode:

$$v_{out} = i_{ph} G_{TIA} = P_{out} R G_{TIA} \tag{3.14}$$

Using equation (3.10) in (3.14), the full relationship between the modulation and the output electrical value can be determined as:

$$v_{out} = \frac{G_{TIA} R P_{in} IL}{2} cos^2\left(\pi v_{BIO}(t)/v_\pi\right). \tag{3.15}$$

Considering a MZI linear operation, i.e. setting $v_{bias} = N\, v_\pi/2$, where n is an odd number, (3.15) can be simplified into:

$$v_{out} = \frac{G_{TIA} R P_{in} IL}{2} \left(\pi v_{BIO}(t)/v_\pi\right). \tag{3.16}$$

Taking into account the skin-interface impedance and the input impedance of the acquisition system as described in Chapter 2, a more complete transfer function of the overall photonic sensor can be derived:

$$v_{out} = \frac{G_{TIA} R P_{in} IL}{2} \left({}^{\pi v_{BIO}(t)}/_{v_{\pi}} \right) \left(\frac{Z_{in}}{Z_{in} + \left[R_{sc} + \frac{R_{ep}}{1 + j\omega C_{ep} R_{ep}} + \frac{R_e}{1 + j\omega C_e R_e} \right]} \right). \quad (3.17)$$

3.4.3 Limitation Factors

For the majority of EO applications, the noise currents in the photodetection stage determine the minimum electric field level that can be detected, i.e. the minimum optical power level. Thus, in order to maximize photodetection sensitivity (photodiode + TIA) it's important to maintain a giving SNR. The SNR is defined as the simplest measure of the quality of reception and is represented as the ratio of the mean square of the power and the sum of the variances of the noise sources. The Carrier-to-noise Ratio (CNR) is the equivalent of the SNR of a modulated or Radiofrequency (RF) signal, and it can be represented by [14, 15]:

$$CNR = \frac{\theta^2}{2} SNR = \frac{carrier\ power}{source + photodiode + TIA}\ , \quad (3.18)$$

where the carrier power (CP) represents the optical power developed at the photodiode. The denominator includes the noises from the source, photodiode and amplifier. The CP can be defined as:

$$CP = \frac{1}{2} \left(\theta R G_{ph} P_{out} \right)^2 \quad (3.19)$$

where G_{ph} is the gain of the photodiode, which in the case of using PIN-based detectors has a unity value [14]. The main noise associated with the source is influenced by the laser relative intensity noise (RIN), which is associated with random spontaneous emissions that influence the laser intensity. The RIN is estimated by the following relationship [14], [16]:

$$RIN = \frac{\langle (\Delta P_{in})^2 \rangle}{P_{in}}, \quad (3.20)$$

where the numerator is the mean square intensity fluctuations of the optical source and the denominator corresponds to the average optical power generated. The overall source noise is defined as:

$$\langle i_{source}^2 \rangle = RIN(RP_{in})^2 BW, \tag{3.21}$$

where BW is the bandwidth.

Regarding the photodiode-related noises, the most important effects result from the statistical nature of the photon-to-electron conversion process, i.e. quantum or shot noise, as well as the dark current (i_{dark}) noise. The overall photodetector noise that contributes to the CNR can be described as [15]:

$$\langle i_{phnoise}^2 \rangle = 2q\left(i_{ph} + i_{dark}\right) BW G_{ph} NF_{ph} \tag{3.22}$$

where NF_{ph} is the noise figure associated with the photodetector, and for PIN diodes $G_{ph}NF_{ph}$ =1.

The remaining limitation factor that contributes to CNR according to (3.18) is the noise associated with the transimpedance stage. This noise is mainly due to thermal effects introduced by the TIA, and can be defined as:

$$\langle i_{TIA}^2 \rangle = \frac{4k_B T}{R_{TIAeq}} BW NF_{TIA}. \tag{3.23}$$

where R_{TIAeq} is the effective resistance load of the photodetector, which in this case represents the TIA, T is the temperature in K, NF_{TIA} is the effective noise figure of the TIA [15].

The CNR is defined according to the main limitation of the system, i.e., the source, photodiode or TIA noise. The general expression for CNR, considering all the noise effects described can be obtained substituting (3.19), (3.21), (3.22) and (3.23) into (3.18), yielding:

$$CNR = \frac{\frac{1}{2}\left(\theta R G_{ph} P_{out}\right)^2}{\left[RIN(RP_{in})^2 BW\right] + \left[2q\left(i_{ph}+i_{dark}\right)BW\right] + \left[\frac{4k_B T}{R_{TIAeq}} BW NF_{TIA}\right]}. \tag{3.24}$$

For maximum sensitivity, the photodiode must be quantum noise limited, i.e. when the quantum noise is higher than the thermal noise. In addition, more simplifications can be made

to (3.24), considering that the effect of the source noise and the dark current are negligible over the shot noise and TIA thermal noise. Therefore, equation (3.24) can be simplified into:

$$CNR = \frac{\theta^2 \eta P_{out}}{2hf_c BW}. \quad (3.25)$$

3.4.4 Performance-driven Parameters

Overall sensor performance is mainly driven by: characteristics of the input optical source (frequency stability and input power), MZI v_π, gain of the current-to-voltage conversion and input impedance of the photonic sensor.

In order to increase overall sensitivity and acquire signals as low as 5 μV, a high P_{in} and a low v_π should be used. The v_π can be reduced by increasing the electrode length, since the EO interaction is augmented, improving the net θ. Nevertheless, there's a limitation regarding the EO modulator settings, since they can't be easily changed after assembly. In fact, opening a sealed MZI modulator could lead to damages in the waveguides due to air particles. Therefore, after designing the photonic sensor and seal the device, the main parameters influencing the overall performance are the P_{in} and G_{TIA}. There's a tradeoff between both parameters, since to compensate the DC levels introduced by a higher optical power, the the TIA components need to have higher values. This results in probable instability of the TIA and higher 50 Hz interference pick-up, due to an increase of the parasitic capacitance. The implemented solution consists in including a DC suppression block when designing the TIA, ensuring the sufficient gain and less probability of saturation. The feedback block low-cut frequency and attenuation depth are selected according to the value of the input optical power. This component will be discussed in Chapter 4.

Another important optimization consideration is to match the properties of the optical signal source used, e.g. wavelength and optical power, with the implemented MZI modulator specifications. In addition, since EO modulation used is based on intensity variations, it's important to prevent optical power oscillations beyond those originated by the bioelectric signal, i.e. minimize RIN.

Table 3.2 includes the main parameters for each component that ultimately influence the overall photonic stage performance.

Table 3.2 Performance-driven parameters for each photonic sensor component.

Element	Parameter	Considerations
Optical Source	P_{in}	As high as possible to improve EO S_{MZI}.
	RIN	As low as possible to avoid artifacts external to bioelectric signal recording.
Photodiode	R	As high as possible to improve conversion efficiency.
	$\langle i^2_{phnoise} \rangle$	As low as possible to improve CNR.
MZI	Z_{in}	Sufficiently high to prevent signal attenuation.
	v_π	As small as possible to increase S_{MZI}.
	IL	This parameter should be improved as much as possible to avoid power losses during EO modulation.

3.5 Evaluation performance

In order to estimate the minimum required settings for the photonic sensor designed, a set of simulations and theoretical calculations can be performed. A direct way to understand the threshold values for each parameter is to analyze the transfer function of the photonic sensor described in (3.17), as well as the CNR (3.24). Some of the parameters involved in these equations can already be defined, as shown in Table 3.3.

Table 3.3 Photonic stage parameters used for theoretical calculations and simulations.

Properties	Value	
Material	$LiNbO_3$	n= 2.208
		$r_p = 30.8 \times 10^{-12}$ m/V
Wavelength	1550 nm ($f_c = 1.9 \times 10^{14}\ Hz$)	
MZI configuration	Dual drive/ Push-pull effect	
Planck Constant	$h = 6.63 \times 10^{-34}\ J.s$	
Electron charge	q = 1.602 x 10^{-19} C	
Bandwidth	BW =1 kHz	

In the following sub-sections theoretical estimations on photonic stage performance, as well as simulations using a photonic-based software will be explored.

3.5.1 Theoretical Calculations

Two different analysis can be performed: either define which is the minimum signal to be detected and re-define the EO sensor parameters according to (3.17); or determine the output voltage according to the pre-set values for each parameter.

Since the purpose of this device is to detect electric field or voltage signals, it's important to define the minimum signal detected according to a specific set of parameters. Therefore, replacing (3.2) in (3.25) and solving the latter for $CNR = 1$, it's possible to find the minimum detectable field, yielding:

$$V_{min} = \frac{\lambda \sqrt{\frac{hf_c BW}{P_{out}\eta}}}{2\pi n^3 r_p} \tag{3.26}$$

The necessary bandwidth for the system can be determined by the maximum frequency component of interest of the bioelectric signals measured. A sufficient bandwidth for the overall system would be 1 kHz, since EMG signals have the higher frequency components (< 500 Hz). However, before defining the minimum detectable field, it's important to set the threshold values for each of the parameters involved in (3.26). Regarding the optical power used, the minimum measured optical power at the photodetector may be calculated through the use the noise equivalent power (NEP). NEP corresponds to the minimum detectable power per square root bandwidth (f_c) and is defined as:

$$NEP = \frac{\langle i_{phnoise}^2 \rangle}{R} = \sqrt{2qP_{out}BW} \tag{3.27}$$

which solved for P_{out} and considering $f_c = 1\ Hz$, yields:

$$P_{out} = \frac{NEP^2}{2qBW} \tag{3.28}$$

After having the minimum input power, as well as defined photonic stage parameters, it's possible to estimate the minimum detectable field, and what would be the expected output for each desired bioelectric signal. Therefore, for the following calculations, some

assumptions need to me made, based on typical values existent in the literature and in typical commercialized devices (Table 3.4).

Table 3.4 Parameters assumptions for theoretical calculations.

Properties	Considerations	Value
Input optical power	Minimize power consumption	100 μW – 10 mW
Half-wave voltage	Minimize sensor dimensions	1 – 6 V
Insertion loss	Minimize losses	6 dB
Responsivity	Optimize the OE conversion efficiency	0.8 A/W
NEP	Allow low power sources	1 x 10^{-12} W/$Hz^{1/2}$
Transimpedance Gain	Optimize the OE conversion efficiency	1 x 10^{5} V/A

The estimation of the minimum input power used in bioelectric signal measurements using the designed photonic stage can then be performed substituting values in Table 3.4. Therefore, the minimum detected power at the photodetection stage is:

$$P_{out} = \frac{(1\times10^{-12})^2}{2 \times 1.602\times10^{-19} \times 1000} = 3.1211\ nW$$

The equivalent input power P_{in} can be determined by subtracting the effect of the insertion loss throughout the MZI modulator:

$$IL = 10log\left(\frac{P_i}{P_{out}}\right) <=> P_i = 3.1211\times10^{-9} \times10^{6/10} = 12.45\ nW.$$

Replacing parameters in (3.26) and considering the calculated minimum detectable optical power, the minimum detectable signal is determined as 0.1884 V, which is almost 40 times greater than the highest amplitude of bioelectric signals, i.e. EMG. However, this v_{min} represents the threshold voltage detected with the worst-case scenario, where the limits of photodetection are tested. If an input optical power in the ranges shown in Table 3.4 is considered, the minimum detected voltage can be increased and reach appropriate values for bioelectric signal acquisition applications. Therefore, considering an input optical power of 10 mW, the incident power at the photodetection stage is 2.5 mW. For this case, the minimum detected field is 210 μV, which is more adequate considering the typical amplitudes of bioelectric signals (5 μ to 10 mV).

Equation (3.16) can be used in order to find the expected output voltages for each type of bioelectric signal detected using pre-set values, or optimized parameters. Table 3.5 shows the results obtained for each bioelectric signal, considering a $P_{in} = 10\ mW$ and $v_\pi = 6\ V$.

Table 3.5 Theoretical output voltage for each bioelectric signal.

Properties	Range input amplitudes	Raw theoretical output voltage
ECG	0.5 – 4 mV	0.5 – 5.0265 V
EEG	5 – 300 µV	0.0063 – 0.3770 V
EMG	0.1 – 10 mV	0.1257 – 12.5664V

An important setting of the photonic stage, especially considering wearable applications, is the aspect ratio of the system, i.e. dimensions. In the case of the MZI modulator itself, this value can be determined through the v_π definition, as described in equation (3.3), although an alteration needs to be performed giving dual drive configuration, yielding:

$$v_\pi = \frac{\lambda d}{2n^3 r_p L}. \tag{3.29}$$

Re-arranging (3.29) in order of the d/L ratio:

$$d/_L = \frac{2n^3 r_p v_\pi}{\lambda} \tag{3.30}$$

The spacing between electrodes in this case corresponds to the spacing between waveguides in the MZI, which isn't related with the electrode position in the body.

3.5.2 Photonic System Simulation

In this section, the main goal is to simulate a specific photonic platform, including also the OE conversion, i.e from an optical modulated signal to a readable output voltage. In this way, its possible to simulate the behavior of the designed photonic platform and verify the threshold voltage detected.

A photonic-based simulation software (OptiSystem 10.0, Optiwave) was used, and the considered setup is shown in Figure 3.7. Although the drive configuration shown here is for the single drive MZI operation, dual drive was also tested, substituting the 0 V signal (Sine Generator 2) by -5 µV.

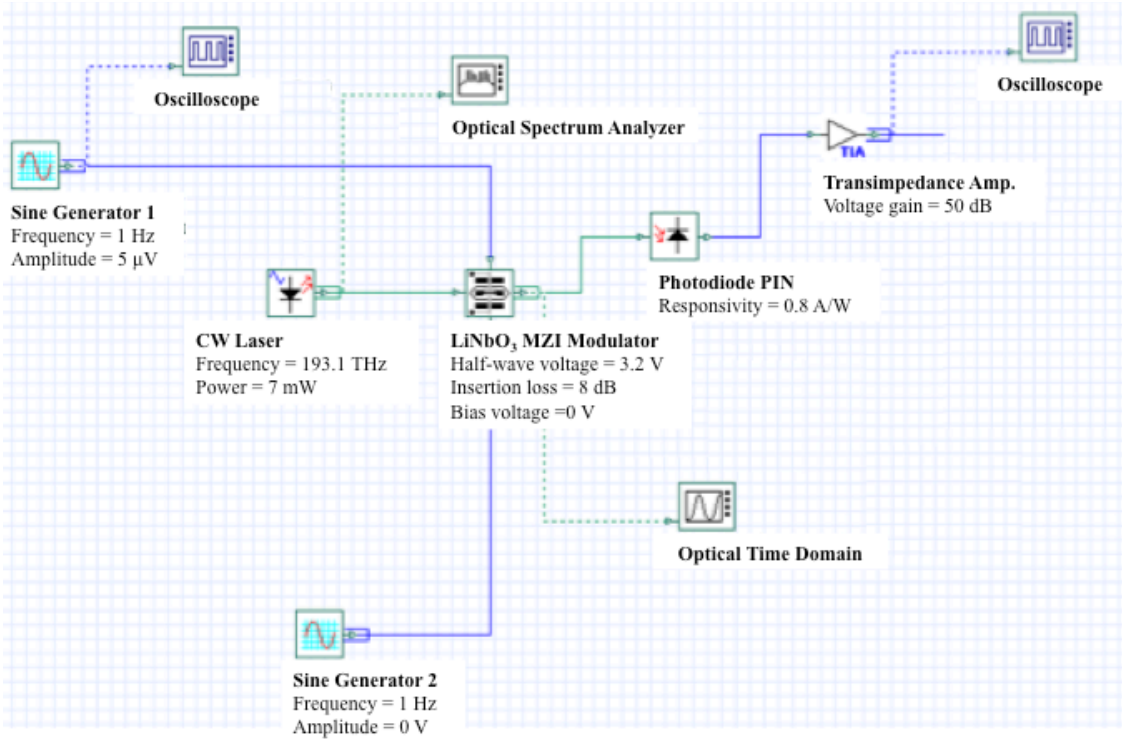

Figure 3.7 Photonic setup used in the simulation software OptiSystems.

As shown in Figure 3.7, the characteristics used for each component are similar to the ones described in Table 3.3 and Table 3.4. The input test signal was a sinusoidal waveform with a peak-to-peak voltage of 10 µV. Results for single drive configuration are shown in Figure 3.8.

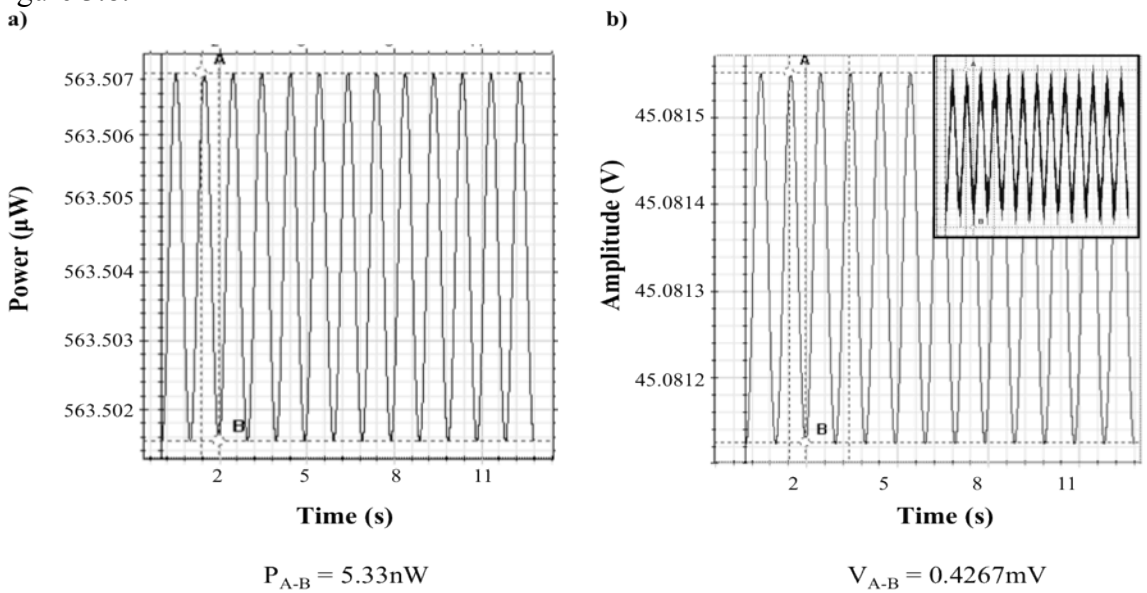

Figure 3.8 Simulation results for MZI single drive configuration, in: a) Optical; and b) Electrical domain. Inset in b) represents the raw signal obtained at the output of the TIA.

The parameters used for dual-drive configuration were the same, although as explained before, a sinusoidal signal equal in amplitude, but with opposite phase, was used to drive the MZI second electrode. Respective results are shown in Figure 3.9.

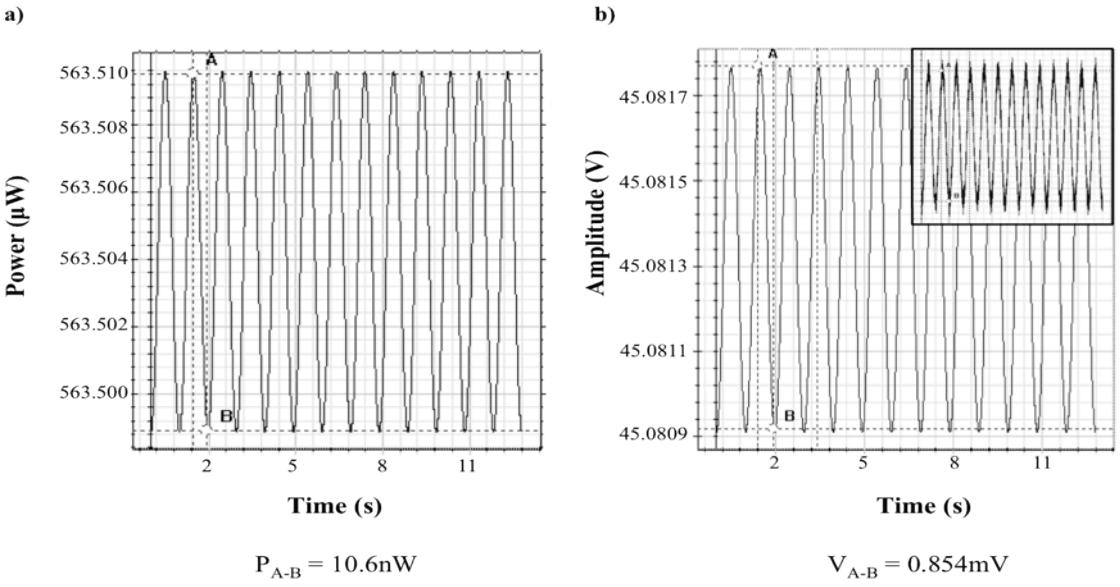

Figure 3.9 Simulation results for MZI dual drive configuration, in: a) Optical; and b) Electrical domain. Inset in b) represents the raw signal obtained at the output of the TIA

Analyzing both results, the effect of dual drive configuration (Figure 3.9) is obvious, resulting in twice the s_{MZI} in respect to single drive (Figure 3.8). Thus, if using a photonic stage with the settings indicated in Figure 3.7, it's possible to achieve satisfactory performances.

3.6 Photonic System Overview

This section presents the overview of the photonic system design. Table 3.6 shows the values for each parameter that determines component selection when designing the prototype for the photonic stage. In addition, these values are important to define the optoelectronic (OE) acquisition setup that will be subject of the next Chapter.

Table 3.6 Photonic System properties overview.

System component	Properties	Value	
Optical Signal Source	Optical input Power	100 μW – 10 mW	
	Wavelength	1550 nm ($f_c = 1.9\times10^{14}\ Hz$)	
MZI Modulator	Material	$LiNbO_3$	n= 2.208
			$r_p = 30.8 \times10^{-12}$ m/V
	Drive configuration	Dual drive/ Push-pull effect	
	Half-wave voltage	1 – 6 V	
	Insertion loss	6 dB	
Photoreceiver	Responsivity	> 0.8 A/W (@1550 nm)	
	NEP	1 x 10^{-12} W/$Hz^{1/2}$	
	TIA Gain	1 x 10^5 V/A	

References

[1] R. W. Waynant and M. N. Ediger, *Electro-Optics Handbook*, vol. 24. McGraw-Hill, 1994.

[2] B. E. A. Saleh and M. C. Teich, *Fundamentals of photonics*, vol. 45, no. 11. Wiley-Interscience, 2007, p. 1177.

[3] C. Shun-Lien, *Physics of photonic devices*, 2nd ed. John Wiley & Sons, 2009.

[4] S. Iezekiel, "Microwave Photonics – an Introductory Overview," in *Microwave Photonics: Devices and Application*, S. Iezekiel, Ed. John Wiley & Sons, Inc., 2009.

[5] G. Lifante, *Integrated photonics: fundamentals*. John Wiley & Sons, 2003.

[6] K. Iizuka, *Elements of photonics - Volume I*, vol. 1. Wiley-Interscience, 2002.

[7] L. Dalton et al., "Polymeric Electro-optic Modulators: From Chromophore Design to Integration with Semiconductor Very Large Scale Integration Electronics and Silica Fiber Optics," *Industrial & Engineering Chemistry Research*, vol. 38, no. 1, pp. 8-33, Jan. 1999.

[8] E. L. Wooten et al., "A review of lithium niobate modulators for fiber-optic communications systems," *IEEE Journal of Selected Topics in Quantum Electronics*, vol. 6, no. 1, pp. 69-82, 2000.

[9] D. Janner, D. Tulli, M. García-Granda, M. Belmonte, and V. Pruneri, "Micro-structured integrated electro-optic LiNbO 3 modulators," *Laser & Photonics Review*, vol. 3, no. 3, pp. 301-313, Apr. 2009.

[10] K. IIzuka, *Elements of Photonics - Volume II*. Wiley-Interscience, 2002.

[11] Y. Fujii, Y. Otsuka, and A. Ikeda, "Lithium Niobate as an Optical Waveguide and Its Application to Integrated Optics," *IEICE Transactions on Electronics*, vol. E90-C, no. 5, pp. 1081-1089, 2007.

[12] X. Wang, H. Tian, and Y. Ji, "Photonic crystal slow light Mach–Zehnder interferometer modulator for optical interconnects," *Journal of Optics*, vol. 12, no. 6. p. 065501, 01-Jun-2010.

[13] L. Kotacka, "Advanced Photonic Components," pp. 1-23.

[14] G. Keiser, "Optical Fiber Communications," *Encyclopedia of Telecommunications*, 2000.

[15] J. G. Graeme, *Photodiode amplifiers*. McGraw-Hill, 1995.

[16] C. DeCusatis and C. DeCusatis, *Fiber Optic Essentials*. Academic Press, 2005.